Department of Diagnostics and Intervention, 2026

Gynecological cancers:

from experimental genetics in mice to the prognostic role of LRIG1 in patients

Alexandra Lorenzzi de Melo

UMEÅ UNIVERSITY

This work is protected by the Swedish Copyright Act (Act 1960:729)
© 2026 Alexandra Lorenzzi de Melo
ISBN: 978-91-8070-892-0 (print)
ISBN: 978-91-8070-893-7 (pdf)
ISSN: 0346-6612
Umeå University Medical Dissertations New Series no. 2402
Cover: Artistic representation of a tree, symbolizing reproduction and continuity at the core of the gynecological tract. Artwork by Cassiano Blanco, used with permission.
Cover reproduced with permission
Electronic version available at: http://umu.diva-portal.org/
Printed by: Scandinavian Print Group, Skarpnäck, 2026

“The more I learn, the more I realize how much I don’t know.”
— Albert Einstein
(A sentence wisely repeated by my beloved grandfather, Dr. Pedro Raposo de Melo)

Table of contents

Abstract ..... **iv**

Original papers ..... **vi**

List of abbreviations ..... **vii**

Acknowledgements ..... **ix**

Introduction **1**
GYNECOLOGICAL CANCER 1
OVARIAN CANCER 1
Epidemiology and Risk factors *2*
Challenging early detection *2*
Histological and Molecular Types *3*
Staging and Treatment *3*
CERVICAL CANCER 4
Epidemiology and Risk Factors *4*
Histological and Molecular Types *5*
Staging and Treatment *5*
Vaccination *6*
ENDOMETRIAL CANCER 7
Epidemiology and Risk Factors *7*
Histological and Molecular Types *7*
Staging and Treatment *8*
LRIG FAMILY AND LRIG1 9
LRIG1 and BMP signaling *10*
LRIG1 and Cancer *11*

Aims **12**

Materials and methods **13**
CLINICAL COHORTS 13
Ovarian Cancer patients cohort (Paper I and III, Cohort #1) *13*
Early-stage ovarian carcinoma (Paper III, Cohort #2) *13*
Low Grade Serous Ovarian Carcinoma (Paper III, Cohort #3) *14*
Cervical Cancer (Paper II, Cohort #4) *14*
Early-stage Endometrial Carcinoma (Paper IV, Cohort #5) *14*
LRIG1 SIMOA ASSAY DEVELOPMENT (PAPER I) 15
IMMUNOHISTOCHEMISTRY (PAPERS II-IV) 16
Antibody Validation (Paper III) *16*

Immunohistochemical staining (Paper II, III, and IV) *18*
IHC Scoring systems *19*
IN VITRO EXPERIMENTS (PAPER V) 19
Ovarian cancer cell lines *19*
Transduction (shRNA human library) *20*
Barcode library generation and transduction *21*
XENOGRAFT MOUSE MODEL FOR OVARIAN CANCER (PAPER V) 21
Animal strain and husbandry *22*
Cell implantation *22*
Chemotherapy treatment *22*
Tumor monitoring *22*
Euthanasia and material collection *22*
DNA extraction and PCR amplification *23*
NEXT-GENERATION SEQUENCING (PAPER V) 24
Bioinformatics analysis *24*
STATISTICAL METHODS 24
Survival Analyses *25*
TCGA gene expression survival analyses (Paper IV) *25*
ETHICAL CONSIDERATIONS 26

Results and Discussion 28
PAPER I 28
MAIN FINDINGS 28
Development and analytical performance of the LRIG1 Simoa assay *28*
LRIG1 plasma levels in ovarian tumor patients *28*
DISCUSSION 29
PAPER II 31
MAIN FINDINGS 31
High LRIG1 expression predicts lymph node metastasis in patients with uterine cervical cancer *31*
DISCUSSION 32
PAPER III 34
MAIN FINDINGS 34
Development and validation of the monoclonal anti-LRIG1 antibody *34*
LRIG1 immunoreactivity in ovarian carcinoma cohorts *34*
Prognostic implications of LRIG1 immunoreactivity *35*
DISCUSSION 36
PAPER IV 39
MAIN FINDINGS 39
BMP signaling regulators and survival in stage I endometrioid endometrial carcinoma *39*
LRIG1 protein expression and prognosis in stage I endometrioid endometrial carcinoma *39*

DISCUSSION 40
PAPER V 43
MAIN FINDINGS 43
Tumour formation across four human ovarian cancer cell lines 43
Effects of chemotherapy 43
Frequency of tumor-initiating cells in the xenograft models 43
DISCUSSION 44

Conclusions 47

References 48

Abstract

Gynecological cancers comprise a heterogeneous group of malignancies arising from the female reproductive tract, most commonly involving the uterus, ovaries, and cervix. Together, they accounted for more than 1.47 million new cases and 680,000 deaths worldwide in 2022, with substantial global disparities in incidence and mortality. Their development reflects a multifactorial interplay of genetic susceptibility, hormonal and metabolic dysregulation, and lifestyle influences. Gynecologic malignancies are biologically heterogeneous diseases, and despite advances in molecular profiling, reliable biomarkers for prognostic evaluation and therapeutic stratification remain limited.

Leucine-rich repeats and immunoglobulin-like domains protein 1 (LRIG1) is a transmembrane protein that functions as a tumor suppressor by regulating receptor tyrosine kinases and promoting bone morphogenetic protein (BMP) signaling. Elevated LRIG1 expression has been linked to favorable prognosis in various human cancers, though its prognostic role in gynecologic malignancies remains under investigation.

Ovarian carcinoma represents the eighth leading cause of cancer-related death among women worldwide, largely due to late-stage diagnosis, high recurrence rates, and treatment resistance. To investigate the role of LRIG1 in biologic fluids, a quantitative LRIG1-specific single-molecule array assay was developed. LRIG1 plasma levels were measured in 486 patients with suspected ovarian masses. Elevated LRIG1 levels correlated with poor prognosis and independently predicted outcomes in stage III ovarian carcinoma, indicating its potential as a biomarker. To further validate its role, a novel monoclonal anti-LRIG1 antibody, named 10C8, was developed. Immunohistochemical analyses across three independent ovarian carcinoma cohorts revealed an inverse correlation between tumor immunoreactivity and plasma levels, and higher LRIG1 expression in malignant versus benign or borderline tumors. However, prognostic significance varied by histological subtype and disease stage, suggesting a context-dependent clinical utility.

Cervical cancer is a major global health concern, with early-stage disease (FIGO IA2–IB1) carrying a risk of lymph node metastasis (LNM) in approximately 15% of patients. The presence of LNM often necessitates combined surgical and radiotherapeutic treatment, which substantially increases morbidity and adverse effects. Current preoperative diagnostic tools lack sufficient sensitivity to accurately predict nodal involvement prior to surgery. In this context, the ability of LRIG1 immunoreactivity to predict LNM was evaluated among 67 early-stage cervical carcinoma cases. This analysis revealed that high LRIG1 expression

correlated with risk of LNM (odds ratio 9.5), suggesting a potential role as a predictive and prognostic biomarker in cervical cancer.

In endometrioid endometrial carcinoma, a subset of early-stage patients experience relapse, underscoring the need for improved prognostic indicators. Transcriptomic analysis of TCGA cases showed that elevated expression of several BMP signal-promoting genes correlated with poorer survival, whereas one BMP signal-suppressing gene was linked to improved outcome. Based on these findings, a tissue microarray of 241 stage I tumors was constructed to evaluate the prognostic relevance of LRIG1 tumor immunoreactivity. No significant association was observed between LRIG1 tumor immunoreactivity and relapse-free survival, though higher LRIG1 staining correlated with increased estrogen receptor, progesterone receptor, and Ki-67 expression.

To identify genes mediating resistance to platinum-taxane based chemotherapy in ovarian carcinoma, a series of human-mouse xenograft models were investigated. Genetic barcode experiments revealed that approximately 500-5,000 tumor-initiating cells contributed to tumor formation in the OVCAR3, OVCAR4, OVCAR8, and OVSAHO xenograft models. These results will guide future efforts to genetically screen for potential treatment targets in chemotherapy-resistant ovarian carcinoma.

Together, these studies provide new insights into the biological and prognostic roles of LRIG1 across major gynecologic cancers.

Original papers

Paper I **de Melo ALL**, Linder A, Sundfeldt K, Lindquist D, Hedman H. Single-molecule array assay reveals the prognostic impact of plasma LRIG1 in ovarian carcinoma. *Acta Oncol*. 2022;61(11):1425-1433. doi:10.1080/0284186X.2022.2140016

Paper II Israelsson P, Lif L, Oda H, **de Melo AL**, Lindquist D, Hedman H. High LRIG1 expression predicts lymph node metastasis in patients with uterine cervical cancer. *FEBS Open Bio*. 2025;15(12):2045-2053. doi:10.1002/2211-5463.70092

Paper III **de Melo AL**, Båtsman M, Linder A, Sundström H, Parris T, Helou K, Lindquist D, Hedman H. LRIG1 immunoreactivity in ovarian carcinoma – inverse correlation with plasma levels, and prognostic implications. Manuscript.

Paper IV **de Melo AL**, Patthey A, Sundström H, Båtsman M, Lindquist D, Hultdin M, Hedman H. Endometrioid endometrial carcinoma stage I: prognostic implications of BMP signal regulators. Manuscript.

Paper V **de Melo AL**, Twayana KS, Smialowska A, Lindquist D, Hedman H. Methodological insights from genomic libraries transductions and in vivo selection in ovarian carcinoma xenograft models. Manuscript.

List of abbreviations

3Rs	Replacement, Reduction, Refinement (principles for animal experiments)
8×His	8× Histidine purification tag
BMP	Bone Morphogenetic Protein
BSL-2	Biosafety Level 2
CA-125	Cancer Antigen 125
CAR-T	Chimeric Antigen Receptor T-cell
CC1	Cell Conditioning Solution 1
CI	Confidence Interval
COS7	CV-1 in Origin, carrying SV40 (African green monkey kidney cell line)
DAB	3,3′-Diaminobenzidine
DFS	Disease-Free Survival
DNA	Deoxyribonucleic Acid
EDTA	Ethylenediaminetetraacetic acid
EGFR	Epidermal Growth Factor Receptor
ELISA	Enzyme-Linked Immunosorbent Assay
ER	Estrogen Receptor
FIGO	International Federation of Gynecology and Obstetrics
HGSC	High-Grade Serous Carcinoma
HR	Hazard Ratio
HRP	Horseradish Peroxidase
IHC	Immunohistochemistry
KLH	Keyhole Limpet Hemocyanin
KRAS	Kirsten Rat Sarcoma Viral Oncogene
LGSC	Low-Grade Serous Carcinoma
LN	Lymph Node
LNM	Lymph Node Metastasis
LRIG	Leucine-rich Repeats and Immunoglobulin-like Domains
LRIG1	Leucine-rich Repeats and Immunoglobulin-like Domains Protein 1
LVSI	Lymphovascular Space Invasion
MAPK	Mitogen-Activated Protein Kinase
MEF	Mouse Embryonic Fibroblast
MOI	Multiplicity of Infection
MSI	Microsatellite Instability
mRNA	Messenger RNA
NBIS	National Bioinformatics Infrastructure Sweden
NGS	Next-Generation Sequencing
NSG	NOD scid gamma
NSMP	No Specific Molecular Profile
OR	Odds Ratio

OS	Overall Survival
PCR	Polymerase Chain Reaction
PD-1	Programmed Cell Death Protein 1
PD-L1	Programmed Death-Ligand 1
pLKO	Lentiviral plasmid backbone
POLE	DNA Polymerase Epsilon
RNA-seq	RNA Sequencing
ROCA	Risk of Ovarian Cancer Algorithm
ROMA	Risk of Ovarian Malignancy Algorithm
sLRIG1	Soluble LRIG1
SDS	Sodium Dodecyl Sulfate
Simoa	Single Molecule Array
SPSS	Statistical Package for the Social Sciences
TGFβ	Transforming Growth Factor Beta
TRC	The RNAi Consortium
UCCB	Umeå Centre for Comparative Biology
UKCTOCS	United Kingdom Collaborative Trial of Ovarian Cancer Screening
VEGF	Vascular Endothelial Growth Factor
VSV-G	Vesicular Stomatitis Virus Glycoprotein

Acknowledgements

I have imagined writing this section countless times over the years. It has always been the first thing I look for when I receive a thesis, and at different moments in my life I pictured what it might feel like to write my own, whether in times of encouragement, excitement, or gratitude. Now, after so many years dedicated to this project and surrounded by such a special group of people, it is impossible not to feel deeply moved.

To our dear LRIG1 group:

It was truly a pleasure to be part of this team, joining the meetings, listening to the discussions, and sharing in the excitement of each new discovery. It is a privilege to witness the work being done around this fascinating protein family.

Pernilla, Mikael, Samuel, and Olla, I learned so much from our weekly meetings, and I deeply appreciate the encouragement, suggestions, and knowledge shared. Annika, Ahmad, and Carl, I cherish our life and work exchanges in the lab, especially in the cell lab, and all the support throughout these years. Lotta, thank you for supporting me with the mice experiments in such a calm and wise way. Your help was incredibly meaningful and allowed me to accomplish so much. Krishna, thank you for your collaboration on the ovarian cancer project, and I hope we can soon have more findings to share.

To Håkan and David:

After one of the most devastating periods of my life, you were the ones who kept me standing. More than that, you gave me the resources, encouragement, and trust I needed to keep going. You valued my work at every step of the way, and I can say with complete honesty that this project would not exist without the two of you. I will be forever grateful.

In addition, this has been the most respectful and healthy work environment I have ever experienced. Håkan, I truly admire your ability to transform ideas into real science in a way that makes everything feel uncomplicated, yet deeply enriching and interesting. David, your clinical knowledge is impressive, and your quick thinking is almost intimidating. I was incredibly lucky to have both of you guiding me through this time.

To my colleagues, including PhD students, postdocs, and members of the department groups:

I know I haven't always been the most interactive person, but I hope you know how much each of you has inspired me through your knowledge, work ethic, and enthusiasm. I am very glad that I became more involved with the Journal Club and had the opportunity to exchange ideas with and mostly learn from all of you – Britta, Nick, Parniyan, Cedric, Tommy, Joshua, Adam, and Ahmad.

I would also like to express how much I appreciate the exchange with the department's groups led by Daniel Öhlund, Jonas Nilsson, and Sophia Harlid, through ORM meetings, office sharing, and countless lab encounters. It is truly a pleasure to work in a place where everyone is willing to help in some way. I would especially like to mention Anette Berglund, who was always ready to assist with our immunohistochemistry analyses, especially during the constant machine struggles.

To Luana Aps and Bruna Porchia:

The time I spent at Imunotera was extremely valuable to me. We know how challenging it can be to work with research in Brazil. It requires immense courage, energy, resources, and perseverance. You have built a splendid body of work and continue to fight daily to keep it going. It is truly impressive, and I am confident you will reach your goal: the commercialization of your HPV vaccine.

To my beloved family and long-time friends:

What would I be without you? Thank you for all the support, love, and laughter. I know how much you have been rooting for me, especially this past year, and I made it through thanks to all of you.

To my son, Gustav:

You are my whole heart. My true life partner. Every time I look into your bright, shining eyes and hear you laugh, or simply say "mamãe," I find the strength to do anything. Te amo! This is for you.

Introduction

Gynecological cancer

Gynecological malignancies represent a heterogeneous group of neoplasms originating from the female reproductive tract, including the endometrium, ovaries, fallopian tubes, cervix, vulva, and vagina. Globally, they account for a substantial proportion of the female cancer burden. According to the Global Burden of Gynecological Cancers 2022 Study, more than 1.47 million women were diagnosed and 680,000 deaths occurred that year, with cervical cancer contributing to nearly half of these cases and deaths (1). Given the biological and clinical heterogeneity of these tumors, accurate staging is essential for essential for prognosis, treatment planning, and comparison of outcomes across studies. To this end, gynecological cancers are commonly staged according to the system developed by the International Federation of Gynecology and Obstetrics (FIGO), which provides a standardized framework based on anatomic disease extent and, increasingly, incorporates histopathologic and molecular features.

The relative distribution of gynecological cancers varies markedly by geography and socioeconomic status. In high-income countries, endometrial cancer has become the most frequent gynecologic malignancy, largely attributed to rising obesity rates and increasing life expectancy, and it typically presents at an early stage with favorable prognosis (2). In contrast, cervical cancer remains the leading gynecologic malignancy in many low- and middle-income countries, reflecting poor access to HPV vaccination, screening, and treatment (3, 4, 5). Ovarian cancer, while comparatively less common, carries the highest case-fatality rate among gynecologic cancers due to its asymptomatic onset, advanced-stage presentation, and acquired chemoresistance, where patients initially respond favorably to chemotherapy but eventually develop resistance to treatment (6, 7, 8).

Ovarian Cancer

Ovarian cancer remains one of the most lethal gynecologic malignancies, largely due to the absence of effective early detection strategies. The disease is often asymptomatic in its initial stages, leading to diagnosis at advanced stages when prognosis is poor. Although ovarian cancer represents a relatively rare tumor compared with endometrial or cervical cancers, it accounts for a disproportionately high share of gynecologic cancer deaths. It is estimated that up to 90% of patients could be cured if the disease were detected while still

confined to the ovaries, yet fewer than 20% are currently diagnosed at this early stage (9, 10).

Epidemiology and Risk factors

Ovarian cancer affects approximately 300,000 women worldwide annually. It is a relatively rare cancer, accounting for 3.4% of all incident cancers in women in 2018 (11). In Sweden, ovarian cancer affects 700 women per year and even though its incidence has been decreasing for the past 30 years the mortality rate has not showed such a strong improvement (12).

Established risk factors include increasing age, family history of ovarian or breast cancer, germline *BRCA1/2* mutations, nulliparity, endometriosis, and use of fertility drugs, while protective factors encompass parity, oral contraceptive use, and tubal ligation (13, 14). The protective effect of oral contraceptives is dose- and duration-dependent, reducing lifetime risk by approximately 30–50 % after five years of use (14, 15). Ongoing research continues to explore the interplay between hormonal, inflammatory, and genetic pathways to improve risk prediction and identify viable targets for early detection and prevention.

Challenging early detection

It remains a clinical challenge in women presenting with a suspicious pelvic mass to distinguish malignant from benign disease, largely because of the lack of disease-specific symptoms. Plasma levels of CA-125 and human epididymis protein 4 (HE4), either individually or in combination, as well as their incorporation with menopausal status in the Risk of Ovarian Malignancy Algorithm (ROMA), are commonly employed to support this discrimination (16, 17). However, the predictive performance of these biomarkers and the ROMA algorithm remains far from optimal.

The United Kingdom Collaborative Trial of Ovarian Cancer Screening (UKCTOCS), the largest and most comprehensive randomized controlled trial to date, followed more than 200,000 postmenopausal women over 16 years. The study evaluated multimodal screening using CA125 interpreted with the Risk of Ovarian Cancer Algorithm (ROCA) followed by ultrasound, ultrasound-only screening, and no screening. While the multimodal screening arm showed a significant shift toward earlier-stage ovarian and tubal cancer diagnoses, this stage shift did not translate into a reduction in disease-specific mortality. These findings are critically important, highlighting that a meaningful mortality benefit may require screening strategies capable of detecting ovarian and tubal cancers at an even earlier stage and in a greater proportion of women (18).

Histological and Molecular Types

Epithelial ovarian carcinomas represent the most common histological subtype of ovarian cancer, accounting for approximately 90% of all ovarian malignancies. They arise from the fallopian tube, epithelial lining of the ovary, or peritoneum and are characterized by substantial histopathological and molecular heterogeneity (19, 20, 21). The epithelial tumors are classified into histopathological subtypes (histotypes) based on the tumor histology and grade. The histotypes of low-grade serous, high-grade serous, mucinous, endometrioid, and clear cell, present different cellular origins, risk factors, somatic mutation profiles, clinical behavior, and prognoses (11, 21, 22). The epithelial tumors can also be classified according to a dualistic model, in which the tumors are divided into type I (low-grade serous, endometrioid, clear cell, and mucinous carcinomas) and type II (high-grade serous and undifferentiated carcinomas) (23).

The most aggressive subtype, high-grade serous ovarian carcinoma, accounts for 90% of the serous carcinomas and two-thirds of all ovarian cancer deaths, since it has often progressed to metastatic disease by the time of diagnosis (24). Molecularly, high-grade serous ovarian carcinomas (HGSOC) almost ubiquitously show *TP53* mutations, but except for that, frequent somatic point mutations in cancer driver genes are uncommon. Rather, HGSOC is characterized by genomic instability and DNA copy number abnormalities (8, 25). Approximately 50% of cases are deficient in homologous DNA repair, including 22% with germ line or somatic mutations in *BRCA1* or *BRCA2* (24-26).

In contrast, low-grade serous carcinoma (LGSC) is characterized by recurrent activating mutations in the MAPK signaling pathway, most commonly involving mutations in *KRAS* or *BRAF*. LGSC generally follows a more indolent clinical course compared with high-grade serous carcinoma; however, it demonstrates limited sensitivity to conventional platinum-based chemotherapy. This inherent chemoresistance has significant therapeutic implications and has led to increasing interest in targeted therapies, including MEK inhibitors, for the management of this distinct ovarian cancer subtype (27, 28).

Staging and Treatment

Ovarian cancer is staged according to the FIGO 2014 classification, which integrates ovarian, fallopian tube, and primary peritoneal carcinomas into a unified system based on the anatomical extent of disease at diagnosis, as determined through comprehensive surgical and pathological assessment. Although residual tumor volume following cytoreductive surgery is not

incorporated into the formal FIGO staging criteria, it remains one of the most powerful prognostic indicators of patient outcome. Consequently, the primary therapeutic goal is to achieve complete macroscopic cytoreduction, as minimal residual disease is consistently associated with improved survival (29, 30).

Following surgery, platinum-based combination chemotherapy, typically including carboplatin and paclitaxel, remains the standard first-line treatment and has formed the foundation of therapy for several decades. The introduction of targeted agents, particularly anti-angiogenic therapies (e.g., bevacizumab) and PARP inhibitors, has significantly improved outcomes, especially in patients with *BRCA1/2* mutations or homologous recombination deficiency (HRD). These agents are now routinely incorporated into first-line or maintenance treatment to extend remission duration and delay recurrence (31, 32).

Despite these advances, chemoresistance, both primary and acquired, remains a central challenge and is responsible for most relapses and poor long-term survival (33, 34). Ongoing research is exploring novel therapeutic modalities, including immunotherapy and CAR-T cell approaches, as potential options for platinum-resistant disease (35).

Cervical Cancer

Epidemiology and Risk Factors

Cervical cancer remains a major contributor to cancer-related mortality among women, particularly in low- and middle-income countries, where access to organized screening and HPV vaccination remains limited. Persistent infection with high-risk human papillomavirus (HPV) types, especially HPV-16 and HPV-18, is the primary etiologic factor, accounting for nearly 70% of all cervical cancer cases worldwide (36, 37). Despite advances in vaccination and screening, the global burden remains high, with over 600,000 new cases and 340,000 deaths annually, disproportionately affecting regions without comprehensive prevention programs (36). The widespread implementation of HPV vaccination and cytology- or HPV-based screening has dramatically reduced incidence in high-income countries, underscoring the preventable nature of this disease. Other risk factors include early sexual activity, multiple sexual partners, smoking, prolonged use of oral contraceptives, and immunosuppression, which facilitate HPV persistence and malignant transformation (36, 38).

Histological and Molecular Types

Cervical cancer comprises distinct histological subtypes with differing biological characteristics. The majority of cases (approximately 70 to 80 percent) are squamous cell carcinomas, typically originating from the transformation zone of the cervix. Adenocarcinomas and adenosquamous carcinomas account for most of the remaining cases and are thought to originate from the glandular epithelium of the endocervical canal. Clinically, adenocarcinomas and adenosquamous carcinomas are more likely to present at an advanced stage, may be less readily detected by cytologic screening, and have been associated in some studies with a less favorable response to radiotherapy compared with squamous cell carcinoma (36-38).

These histotypes differ not only in their site of origin but also in their underlying molecular mechanisms and patterns of disease progression. High-risk HPV infection is a critical driver of cervical carcinogenesis. The viral E6 and E7 oncoproteins promote malignant transformation by inactivating the tumor suppressor proteins p53 and retinoblastoma, leading to dysregulated cell cycle progression, genomic instability, and evasion of immune surveillance (37). While HPV-driven oncogenesis is common to both major histological types, additional somatic mutations define molecular diversity and influence clinical behavior.

Among these alterations, *PIK3CA* mutations, observed in approximately one-third of both types of cervical cancer, lead to activation of the PI3K/AKT/mTOR signaling pathway and have been linked to poorer prognosis. *KRAS* mutations occur predominantly in adenocarcinomas, whereas alterations in *EGFR* are more common in squamous cell carcinomas, reflecting distinct molecular pathways underlying each subtype (37, 39). These differences contribute to biological heterogeneity and may help guide future subtype-specific therapeutic strategies.

Staging and Treatment

Management of cervical cancer is based on the FIGO 2018 staging system, which takes into account tumor size, spread to nearby supporting tissues around the cervix (parametrial involvement), and lymph node status to better predict outcomes (38). Early-stage disease (FIGO IA to IB1) is usually treated with surgery. In selected patients who wish to preserve fertility, less extensive procedures may be considered. Conization involves removing a cone-shaped piece of tissue from the cervix that contains the cancer and is used for very early disease. Radical trachelectomy is a fertility-sparing surgery in which the cervix and surrounding tissues are removed while the uterus is left in place, allowing the possibility of future pregnancy. Locally advanced disease (FIGO IB2 to

IVA) is most often treated with a combination of chemotherapy and radiation therapy given at the same time, followed by brachytherapy, a form of internal radiation therapy in which a radiation source is placed directly into or near the cervix to deliver a high dose of radiation to the tumor while limiting exposure to surrounding organs. This combined approach remains the standard treatment with curative intent (38, 40–42). For recurrent or metastatic cervical cancer, treatment options have expanded in recent years. These include targeted therapies such as the anti-angiogenic drug bevacizumab, which inhibits tumor blood vessel formation, and immunotherapies that block the PD-1/PD-L1 pathway, helping the immune system recognize and attack cancer cells. Both approaches have been shown to improve survival in advanced disease (38, 41).

A major change introduced in the FIGO 2018 classification was the inclusion of lymph node metastasis as a staging criterion, reflecting its strong prognostic value (38, 42). Pelvic lymph node involvement is now classified as stage IIIC1, while para-aortic lymph node involvement is classified as stage IIIC2, irrespective of primary tumor size or local extension. Lymph node involvement is associated with a substantial reduction in five-year survival, often in the range of 30 to 50 per cent, particularly in cases with para-aortic nodal metastasis or bulky nodal disease (38, 42-44).

When lymph node metastasis is detected preoperatively, primary chemoradiotherapy is generally preferred over radical surgery, since both approaches offer similar oncological outcomes. However, if surgery is performed and lymph node metastasis is only detected postoperatively, adjuvant chemoradiotherapy is required. Although this combined approach results in comparable survival rates, it is associated with significantly increased treatment-related morbidity (45, 46). Therefore, accurate preoperative identification of lymph node involvement is essential to support optimal treatment selection and reduce the risk of overtreatment.

Vaccination

Equally critical to disease control is primary prevention through human papillomavirus (HPV) vaccination, which targets the oncogenic viral types responsible for the vast majority of cervical cancers. The bivalent, quadrivalent, and nonavalent HPV vaccines provide strong and long-lasting protection against high-risk strains, particularly HPV-16 and HPV-18, and newer formulations also protect against additional carcinogenic genotypes (36, 38, 41). Large-scale studies have demonstrated that vaccination before sexual debut reduces high-grade cervical intraepithelial neoplasia by over 80% and substantially lowers cervical cancer incidence (36, 38, 41). The WHO global strategy aims to achieve 90% vaccine coverage among girls by age 15, alongside screening and

treatment targets, with the goal of eliminating cervical cancer as a public health problem by 2030 (47).

Vaccination complements, rather than replaces, secondary prevention through screening and early detection. Implementation of HPV-DNA testing, alone or in combination with cytology, allows earlier identification of high-risk infections and preinvasive lesions, further reducing incidence. Together, vaccination, organized screening, and stage-appropriate treatment constitute a comprehensive and effective continuum of cervical cancer control that is gradually reshaping global disease patterns (1, 36).

Endometrial Cancer

Epidemiology and Risk Factors

Endometrial cancer is the most prevalent gynecologic malignancy in high-income countries, with incidence rates continuing to increase. The disease typically presents at an early stage due to the hallmark symptom of abnormal vaginal bleeding, resulting in a relatively high survival rate (48). Globally, uterine cancer ranks sixth among cancers in women and fourteenth overall, with more than 380,000 new cases reported in 2018 (49). Rising incidence parallels trends in obesity, population aging, metabolic syndrome, and diabetes, which are the most important modifiable risk factors (48, 50-52). Additional risks include nulliparity, early menarche, late menopause, use of unopposed estrogen, and Lynch syndrome (52).

At diagnosis, roughly 80% of endometrial carcinomas remain localized to the uterus, largely because early bleeding symptoms facilitate detection before extrauterine spread, improving prognosis and treatment outcomes (48). However, recent data show that mortality has increased by approximately 1.9% annually, reflecting a shift toward more aggressive histologic and molecular subtypes and delayed diagnoses in certain populations (50, 53).

Histological and Molecular Types

Endometrial cancer originates from the epithelial lining of the uterine corpus and displays considerable heterogeneity in both morphology and molecular features. Traditionally, it has been categorized into two major histological subtypes: endometrioid and non-endometrioid carcinoma. The endometrioid subtype, which accounts for approximately 75–80% of all cases, is typically estrogen-dependent, of low-grade, and it is often detected at an early stage due to the early onset of abnormal uterine bleeding. This form of the disease is associated with a favorable prognosis and a high cure rate when managed appropriately (48-52). In contrast, non-endometrioid carcinomas, comprising

serous, clear cell, mixed histologies, and carcinosarcomas, are generally estrogen-independent, exhibit high-grade nuclear atypia and chromosomal instability, and tend to present at advanced stages. These tumors are biologically aggressive and confer a significantly poorer prognosis, accounting for a disproportionate share of endometrial cancer–related mortality despite their lower incidence (52-54).

In recent years, advances in genomic research have fundamentally redefined the understanding of endometrial cancer biology. The landmark analysis conducted by The Cancer Genome Atlas (TCGA) established a molecular classification system that stratifies endometrial carcinomas into four distinct subgroups with unique genomic alterations, prognostic profiles, and therapeutic implications. The POLE-ultramutated group stands for tumors harboring pathogenic mutations in the exonuclease (proofreading) domain of the *POLE* gene and is characterized by an exceptionally high mutational burden, strong immune activation, and an excellent prognosis. The mismatch repair–deficient (MMRd/MSI-high) subgroup demonstrates a hypermutated phenotype and an intermediate prognosis, often associated with increased immunogenicity and potential responsiveness to immune checkpoint inhibitors. The p53-abnormal (copy-number high) subgroup is characterized by ubiquitous *TP53* mutations, most commonly missense point mutations, together with widespread somatic gene copy-number alterations, conferring a serous-like phenotype, marked genomic instability, and poor prognosis. Finally, the no specific molecular profile (NSMP) subgroup encompasses a heterogeneous collection of tumors with variable outcomes that depend on additional histologic and clinical factors. Recently, this subgroup has been further stratified into NSMP estrogen receptor (ER)–positive and ER-negative tumors, a distinction that carries significant implications for prognosis and treatment strategies (55-57).

Staging and Treatment

The 2023 FIGO revision represents a major step forward in the staging of endometrial cancer, introducing an integrated framework that unites molecular, histopathologic, and anatomic parameters to achieve a more precise assessment of prognosis and to inform individualized treatment decisions (52, 55-57). This modern approach acknowledges that variables such as lymphovascular space invasion (LVSI), histologic subtype, and nodal involvement act in concert to influence recurrence risk and survival outcomes. By combining traditional morphologic assessment with molecular insights, the updated staging system supports a more refined stratification of patients and enables the tailoring of therapeutic intensity to biological behaviour (52).

The TCGA molecular classification has been translated into clinical practice through the ProMisE (Proactive Molecular Risk Classifier for Endometrial Cancer) system. ProMisE categorizes endometrial cancers into four prognostic subgroups (POLE-mutated, MMR-deficient, p53 wild-type, and p53 abnormal) and now serves as a foundation for treatment planning (55-57). Tumors with POLE-ultramutated profiles, defined by an exceptionally high mutational burden and robust immune activation, are associated with an excellent prognosis and can often safely omit adjuvant therapy, thereby minimizing overtreatment. In contrast, p53-abnormal cancers, which display high genomic instability and aggressive biological behavior, carry a markedly increased risk of recurrence and typically require multimodal adjuvant therapy combining chemotherapy and radiotherapy. Tumors with MMR deficiency (MSI-high) or NSMP fall between these extremes, and their management is guided by additional clinicopathologic factors such as tumor grade, depth of myometrial invasion, ER expression, and the presence or absence of LVSI (52, 55-57).

Comprehensive surgical staging remains a central component of disease management, providing critical diagnostic and prognostic information. The adoption of sentinel lymph node mapping has markedly improved the accuracy of nodal assessment while reducing the morbidity associated with full lymphadenectomy (52). Postoperative treatment is now increasingly risk-adapted, aligning the extent of adjuvant therapy with the tumor's molecular and histologic characteristics. This strategy seeks to balance oncologic efficacy with quality-of-life preservation, ensuring that patients at low risk of recurrence avoid unnecessary systemic therapy, while those with aggressive molecular features receive appropriately intensified treatment. The integration of molecular classification into staging and therapeutic decision-making thus exemplifies the transition of endometrial cancer care into the era of personalized, evidence-based medicine.

LRIG Family and LRIG1

The human leucine-rich repeats and immunoglobulin-like domains (LRIG) gene family comprises three genes, *LRIG1*, *LRIG2*, and *LRIG3*, which encode three structurally similar transmembrane proteins (58). These proteins are evolutionarily conserved and regulate a wide range of biological processes, including cell growth, differentiation, and metabolism. Among them, LRIG1 has been most extensively studied and is well established as a tumor suppressor in several tissues and organs, including the gastrointestinal tract and brain (59, 60).

Although the exact mechanisms behind LRIG1's tumor-suppressive function are not fully understood, it is known that LRIG1 negatively regulates several oncogenic receptor tyrosine kinases, including the epidermal growth factor receptor, platelet-derived growth factor receptors, MET, RET, and TRKB (61). LRIG1 binds to these receptors and facilitates their ubiquitination and lysosomal degradation, or prevents their ligand-induced activation, thereby attenuating downstream mitogenic signaling (61-63).

Importantly, LRIG1 can be shed from the cell surface, releasing its extracellular or lumenal domain as a soluble protein (sLRIG1). This soluble protein retains biological activity and has been shown to inhibit EGFR signaling, thereby suppressing tumor cell proliferation and migration (61). The ability of LRIG1 to function both at the membrane and as a soluble antagonist suggests that it may influence signaling not only within cells but also in the surrounding microenvironment.

The expression of LRIG1 has also been linked to cellular chemosensitivity, and its downregulation is associated with chemoresistance (64-67). It has been previously described an LRIG1-centered protein-interaction network that regulates growth factor receptor levels (68). This network includes several proteins that potentially could serve as therapeutic targets in human cancers. For example, in ovarian cancer, GAL3ST1 and related sulfatides are elevated (69), while PON2 has been suggested to function as a tumor suppressor in the early stages of the disease (70).

LRIG1 and BMP signaling

LRIG1 also regulates bone morphogenetic protein (BMP) signaling, which plays a central role in differentiation and stem cell regulation. Using Lrig-null mouse embryonic fibroblasts (MEFs), Herdenberg et al. (2021) demonstrated that cells lacking all three LRIG genes exhibit a marked deficiency in BMP signaling and adipogenesis, while reintroduction of LRIG1 or LRIG3, but not LRIG2, restored normal BMP sensitivity (71). The same study also revealed that human LRIG1 variants are associated with increased body mass index but reduced risk of type 2 diabetes, suggesting a role in lipid metabolism and metabolic homeostasis (71). LRIG1 has also emerged as a regulator of stem cell quiescence in multiple tissues. LRIG1 expression marks slow-cycling, long-lived stem cell populations in the skin, oral mucosa, intestine, brain, and mouse incisors, where it maintains these cells in a dormant state (72).

BMPs comprise a subfamily of the transforming growth factor beta (TGFβ) superfamily of ligands. Abdullah et al. (2023), showed that LRIG proteins regulate multiple members of the TGFβ superfamily in a ligand-specific manner

(73). Moreover, the interaction between LRIG and BMP pathways is influenced by other extracellular regulators. Abdullah et al. (2021) identified netrin-1, a secreted protein best known for its role in axon guidance and cancer progression, as a suppressor of BMP signaling that directly antagonizes LRIG-mediated BMP activation through the receptor neogenin (74).

LRIG1 and Cancer

The *LRIG1* gene, transcript, and protein are prognostic factors in several cancer types. High *LRIG1* expression generally correlates with favorable outcomes, including in breast cancer (mRNA) (75), uterine cervical cancer (immunoreactivity) (76, 77), cutaneous squamous cell carcinoma (immunoreactivity) (78), nasopharyngeal cancer (immunoreactivity) (79), oropharyngeal cancer (immunoreactivity) (80), non-small-cell lung cancer (mRNA and immunoreactivity) (81), and hepatocellular carcinoma (immunoreactivity) (82).

In a genome-wide meta-analysis of prognostic markers in ovarian cancer, Willis et al. (2016) showed that high *LRIG1* tumor mRNA expression is associated with longer survival in serous ovarian carcinoma (83). These results suggest that both membrane-bound and shed LRIG1 forms may hold prognostic or diagnostic potential.

As discussed above, high-grade serous ovarian carcinoma often initially responds to carboplatin–paclitaxel treatment but recurs due to chemoresistance. In this context, it is notable that *LRIG1* has been reported to increase cellular sensitivity to platinum-based drugs (64-67). Furthermore, in paclitaxel- and topotecan-resistant ovarian cancer cell lines, PTPRK, a member of the LRIG1-associated protein network, is downregulated (84). Together, these findings suggest that LRIG1 and its network components could serve as biomarkers or therapeutic targets in treatment-resistant ovarian cancer.

Aims

Our general aim was to evaluate the possible role of LRIG1 in gynecological cancers, assessing its prognostic value and association with relevant clinical parameters, and to develop a translatable in vivo model of high-grade serous ovarian carcinoma.

Specific aims:

To develop a detection method for LRIG1 in plasma samples to investigate the prognostic significance in ovarian cancer.

To isolate and characterize a monoclonal LRIG1 antibody suitable for immunohistochemistry in human tissues.

To evaluate the prognostic significance of LRIG1 immunoreactivity in gynecological cancers

To develop a xenograft mouse model for ovarian cancer

To assess the feasibility and biological limits of genomic screening in intraperitoneal ovarian cancer xenografts.

Materials and methods

Clinical Cohorts

In the present work, we analyzed five distinct cohorts to investigate the role of LRIG1 in gynecological malignancies. Our initial analyses focused on ovarian tumors, and as the study progressed, the accumulating findings enabled the expansion of the research to additional disease entities. Consequently, endometrial and cervical cancer cohorts were incorporated, along with analyses of LRIG1 detection in both tumor tissues using immunohistochemistry and in plasma samples. In total, this study comprises data from more than 1,000 patients, all analyzed using comparable protocols and statistical methodologies, which are described in detail later in this section. The clinical characteristics and analyses of each cohort are presented separately below.

Ovarian Cancer patients cohort (Paper I and III, Cohort #1)

Cohort #1 comprised 496 patients who presented an ovarian tumor. Of these patients, 155 patients had benign diseases of the ovary, 73 had borderline-type tumors, 224 had malignant ovarian tumors, and 34 had ovary-localized metastases. In collaboration with Karin Sundfeldt's group from Gothenburg University, we analyzed LRIG1 plasma levels and LRIG1 tumor immunoreactivity from all patients. We obtained ovarian cancer tissue microarray samples from 430 patients. The tissue microarrays were constructed from cases collected from the Sahlgrenska Gynecology Tumor Bank, as described in Barone et al, (2020) (85). Each case was represented by three replicates from 1 mm cylindrical core biopsies.

Early-stage ovarian carcinoma (Paper III, Cohort #2)

Cohort #2 comprised 205 early stage (stage I and II) primary invasive ovarian carcinoma patients diagnosed between 1994 and 2006. The cohort included 94 high-grade serous, 46 endometrioid, 37 clear cell, and 28 mucinous carcinomas. The material was collected by Khalil Helou, University of Gothenburg and it was previously described by Engqvist et al (2018) (86). Full-face formalin-fixed paraffin-embedded specimens were obtained from the Departments of Clinical Pathology at hospitals in Western Sweden. From the 206 cases analyzed by immunohistochemistry, 95 tumors were previously analyzed by RNA-seq. We obtained the LRIG1 mRNA expression (log2-transformed counts) and assessed its association with LRIG1 protein levels (H-score) using Spearman's rank correlation.

Low Grade Serous Ovarian Carcinoma (Paper III, Cohort #3)

We performed immunohistochemistry analysis using tissue microarrays from a specific population cohort from The Canadian Ovarian Experimental Unified Resource (COEUR). This retrospective cohort was created from twelve ovarian cancer biobanks in Canada (Le Page et al, 2018) (87). In the present study, we analyzed a subpopulation of exclusively Low Grade Serous Ovarian Carcinoma patients (n=70), after formally requesting these samples from the COEUR sample's repository.

Cervical Cancer (Paper II, Cohort #4)

In paper II, the study included women with uterine cervical cancer (ICD C53.9) who underwent Wertheim-Meigs operation (radical hysterectomy and pelvic lymph node dissection) at Umeå University Hospital between 1997 and 2021. The patients were identified through patient records and selected according to lymph node status, with the required sample size for statistical power calculated using a 5% significance level (n=67).

Early-stage Endometrial Carcinoma (Paper IV, Cohort #5)

In Paper IV, we assembled a tissue microarray with samples collected from surgical specimens of 271 patients diagnosed with endometrial carcinoma with FIGO stages I-II between 1997 and 2010 at the Department of Pathology, University Hospital, Umeå, Sweden. The original histopathological slides were reviewed by a pathologist (Annika Patthey) and histological parameters were recorded including histological tumor type, presence of deep myometrial invasion (FIGO stage IB), cervical involvement (FIGO stage II), histological FIGO differentiation grade and presence of LVSI. Medical records were reviewed, and clinical data were extracted including treatment protocol, incidence of local recurrence, incidence of metastasis, time of death, and cause of death. 241 samples were included in the final study after cases were excluded due to non-endometrioid subtype (n = 12), and uninterpretable immunohistochemical staining due to artifacts, necrosis or non-represented tumor cells (n = 15). Stage II patients were excluded from the study due to the limited number of cases (n=3), and the analysis was therefore focused on stage I patients to ensure a more representative cohort. Three patients were missing data regarding relapse; therefore they were not considered for survival analysis (n=238), but included for correlation analysis (n=241).

LRIG1 Simoa Assay Development (Paper I)

A Single Molecule Array (Simoa) assay for LRIG1 detection in plasma was developed using the Homebrew Assay Development Kit (Quanterix Corporation, Billerica, MA, USA). The in-house–developed mouse monoclonal antibody 3F7, directed against the immunoglobulin-like domains of human LRIG1, was employed as the capture antibody. A 0.2 mg/mL solution of 3F7 was conjugated to paramagnetic beads by incubation with 0.3 mg/mL 1-ethyl-3-(3-dimethylaminopropyl)carbodiimide at 4 °C. The mouse monoclonal antibody 2B7, recognizing the leucine-rich repeat domain of human LRIG1, was used as the detector antibody and biotinylated at a 40:1 molar ratio of biotin to antibody.

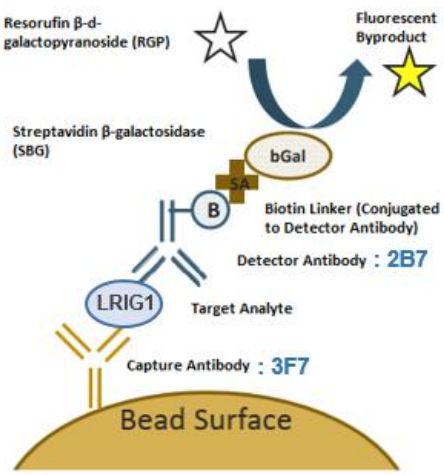

Figure 1 - Single Molecule Array (Simoa) assay representation. (Image adapted from Quanterix)

For assay optimization, recombinant human soluble LRIG1 (sLRIG1) was used as the analyte and for plasma spike experiments. Recombinant sLRIG1 comprised the extracellular/luminal portion of human LRIG1 (GenBank accession no. AF381545; amino acids 35–792) fused to a FLAG and 8×His tag. The protein was expressed in HEK293 cells and purified by immobilized metal affinity chromatography using a Ni-Sepharose Excel column (GE Healthcare, Uppsala, Sweden), yielding a final purity exceeding 90%, as assessed by Coomassie blue–stained SDS–polyacrylamide gels.

The final optimized assay employed a two-step Simoa protocol. Briefly, 300,000 beads conjugated with the 3F7 capture antibody were incubated with diluted samples together with 0.15 µg/mL biotinylated 2B7 detector antibody for 35 min, followed by incubation with 150 pM β-galactosidase–conjugated streptavidin for 5 min. Resorufin β-galactopyranoside was used as the

fluorogenic substrate. All reactions were performed on an HD-1 Simoa analyzer (Quanterix Corporation) according to the manufacturer's instructions.

Assay performance was characterized in terms of dilutional linearity, spike recovery, and specificity. Dilutional linearity was assessed using three different EDTA plasma samples, either unspiked or spiked with 2 ng/mL sLRIG1, and serially diluted twofold from 2× to 32×. Linearity was calculated as: *% Linearity (from X dilution) = (dilution corrected concentration of sample at Y dilution)/(dilution corrected concentration of sample at X dilution)*. The percentage of spike recovery was calculated as *% Recovery = (concentration of spiked sample – concentration of unspiked sample)/(concentration of spike level)*. Specificity was evaluated by measuring the inhibition of assay signal in four EDTA plasma samples following addition of a 20-fold molar excess of unlabelled detector antibody, according to: *% Inhibition = (assay signal in sample with no spike – assay signal in sample spiked with excess of unlabelled detector antibody)/(assay signal in sample with no spike)*.

Validation of LRIG1 detection in the plasma (Paper I)

To evaluate the detectability of LRIG1 in human plasma using the newly developed Simoa assay and to assess potential effects of anticoagulant choice, blood samples were collected from 13 apparently healthy, anonymous volunteers using EDTA or citrate as anticoagulants. Both EDTA and citrate plasma were prepared from each donor. All samples were collected anonymously and in a blinded manner; no personal data were recorded, and none of the donors had any known disease at the time of sampling.

LRIG1 concentrations were measured using the LRIG1 Simoa assay, and paired EDTA and citrate plasma values were compared for each donor. To assess LRIG1 stability, EDTA blood was processed immediately after collection (control) or after storage at room temperature for 4 h or at 4 °C for 24 h before plasma preparation. Plasma stability was further examined by storing EDTA plasma samples at room temperature for 1, 24, or 72 h prior to analysis. The effects of repeated freeze–thaw cycles were evaluated by subjecting EDTA plasma aliquots to 1, 2, 4, or 6 additional freeze–thaw cycles before measurement.

Immunohistochemistry (Papers II-IV)

Antibody Validation (Paper III)

To generate a monoclonal antibody suitable for IHC, we developed the mouse monoclonal antibody 10C8, which recognizes a region within the cytosolic

domain of the LRIG1 protein. A synthetic peptide corresponding to the LRIG1 cytosolic amino-acid sequence NH_2-EPGGSDQEHSPHHQC-COOH was synthesized and conjugated to keyhole limpet hemocyanin (KLH) to enhance immunogenicity. Mice were immunized with the peptide–KLH conjugate following standard hybridoma production protocols. Serum antibody titers from immunized mice were measured by enzyme-linked immunosorbent assay (ELISA) to assess the immune response to the target peptide, and reactive sera were further analyzed by Western blotting to confirm recognition of the LRIG1 protein.

Spleens from mice with the highest antibody titers were collected, and splenocytes were fused with P3X63Ag8.653 mouse myeloma cells using polyethylene glycol to generate hybridoma cell lines. The resulting hybridomas were screened by ELISA for secretion of antibodies reactive to the LRIG1 peptide. ELISA-positive hybridoma clones were subsequently evaluated by Western blotting using lysates from LRIG1-transfected COS7 cells to confirm specificity for the native LRIG1 antigen.

To validate the 10C8 antibody for IHC, formalin-fixed paraffin-embedded cell blocks were prepared using cell pellets from LRIG1-null and LRIG1-inducible HEK293T cell lines. LRIG1-null human embryonic kidney (HEK293T) cells were generated by CRISPR/Cas9-mediated deletion of the entire LRIG1 gene. These knockout cells were subsequently transduced with doxycycline-inducible LRIG1 expression vectors, as described by Faraz et al. (2018). LRIG1 expression was induced by treatment with doxycycline (1 µg/mL) for 24 hours. The LRIG1-null cells served as negative controls, whereas the doxycycline-induced LRIG1-expressing cells served as positive controls for antibody validation. Sections 4 µm thick were cut from the formalin-fixed paraffin-embedded cell blocks using a microtome, mounted on positively charged glass slides, and baked at 60 °C for 1 hour prior to immunohistochemical staining.

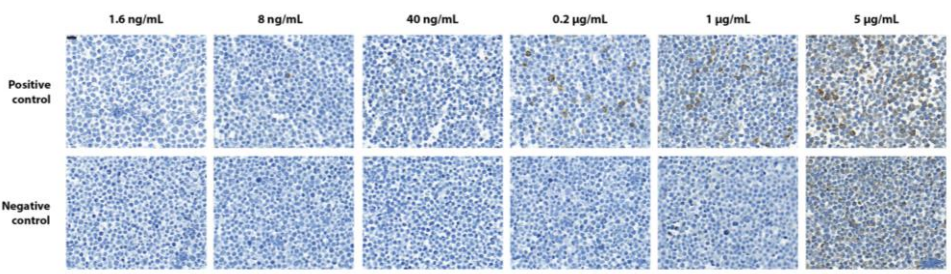

Figure 2 - Monoclonal antibody 10C8 validation using negative and positive controls (figure duplicated from Paper III).

Immunohistochemical staining (Paper II, III, and IV)

Immunohistochemical (IHC) staining was performed on a Ventana BenchMark Ultra automated stainer (Ventana Medical Systems, Tucson, AZ) using the ultraView Universal DAB Detection Kit (Cat. No. 760-500; Roche Diagnostics, Rev J, 2022), a biotin-free detection system. The kit employs a cocktail of horseradish peroxidase (HRP)-labeled secondary antibodies (goat anti-mouse IgG, goat anti-mouse IgM, and goat anti-rabbit IgG) that bind specifically to the primary antibody. Antibody-antigen complexes are visualized through the enzymatic conversion of 3,3′-diaminobenzidine tetrahydrochloride (DAB) in the presence of hydrogen peroxide, forming an insoluble brown precipitate at the antigen site, which is subsequently enhanced with a copper sulfate solution to stabilize and intensify the chromogenic signal.

Tissue sections were automatically deparaffinized using EZ Prep solution (Cat. No. 950-102) and subjected to heat-induced epitope retrieval in Cell Conditioning Solution 1 (CC1, pH 8.5; Cat. No. 950-124) for 36 minutes at 95 °C. Endogenous peroxidase activity was blocked by using the ultraView Universal Inhibitor containing 3% hydrogen peroxide for 4 minutes at 37 °C. The LRIG1 antibody at proper concentration was manually dispensed and incubated for 32 minutes at 37 °C under a liquid coverslip barrier to maintain reagent stability and prevent evaporation. Detection then proceeded automatically through sequential application of the ultraView HRP Multimer, the ultraView DAB chromogen, the ultraView DAB H_2O_2 substrate, and finally the ultraView Copper solution to achieve optimal signal development.

After chromogen development, slides were counterstained with Hematoxylin II (Cat. No. 790-2208) for 20 minutes, followed by Bluing Reagent (Cat. No. 760-2037) for 8 minutes. All reagent incubations, wash steps, and liquid coverslip applications were fully automated by the BenchMark Ultra platform. Upon completion of the staining run, slides were washed gently in a mild detergent solution to remove the liquid coverslip, rinsed in distilled water, dehydrated through graded alcohols, cleared in xylene, and permanently mounted with a resin-based mounting medium.

In Paper II, LRIG1 was detected using the polyclonal antibody Vina at a concentration of 1 µg/mL. In Papers III and IV, the monoclonal antibody 10C8 was used at the same concentration. Both positive and negative control tissues were included in each staining run to ensure assay quality and validity. All slides were scanned using the PANNORAMIC 250 Flash III system (3DHISTECH, Hungary).

IHC Scoring systems

In Paper II, LRIG1 immunostainings were evaluated and interpreted by a pathologist subspecialized in gynecological oncology (Husam Oda), blinded to clinical data and outcomes. LRIG1 expression was quantified by the percentage of cells staining positive (absent, 1-25%, 26-50%, 51-75%, or 76-100%) and staining intensity (none, low, intermediate, or high). Samples were scored as p16-positive if they showed strong and consistent expression in both the nucleus and cytoplasm in over 70% of the cells.

In Paper III, the scoring of LRIG1 staining was performed by two certified pathologists. The final score was based on intensity and amount of stained cells, in which every tissue core was individually evaluated. The intensity of the staining was considered: negative (0), weak (1), moderate (2) and strong (3). The proportion of malignant cells staining positively throughout the section was assigned scores from 0 to 3 (0 <5% positive cells, 1 = 5–10% positive cells, 2 = 11–50% positive cells, 3 >51% positive cells).

In Paper IV, the scoring system was decided before the start of the project and took into consideration both staining intensity and the fraction of stained cells. Intensity was given a score of 0, 1, or 2 where 0 represented no staining, 1 represented weak staining defined as unequivocal staining emerging at 10x magnification, and 2 represented strong staining defined as unequivocal staining at 2x magnification. The fraction of stained cells was accordingly scored 0, 1, or 2 where 0 represented no staining, 1 represented less than 50% stained tumor cells, and 2 represented more than 50% stained tumor cells. If there were different areas of both weak and strong staining in the same sample, only the strongly stained cells were considered when calculating the fraction. The combined LRIG1 score was obtained by adding the intensity score to the fraction score for each sample, thus yielding a total of four categories with the summed scores of 0, 2, 3, or 4. In the cases that initially were scored differently by the two pathologists, the final score was settled through a consensus discussion.

In vitro experiments (Paper V)

Ovarian cancer cell lines

To ensure that our experimental models closely resembled high-grade serous ovarian carcinoma (HGSC), we selected the ovarian cancer cell lines OVCAR8, OVCAR4, OVCAR3, and OVSAHO. This choice was guided by the comprehensive genomic analysis of 47 cell lines believed to originate from HGSC tumors (24). Their analysis, which integrated gene copy-number alterations, somatic mutations, and mRNA expression data, revealed that these

four cell lines recapitulate the molecular characteristics of HGSC tumors. Specifically, OVCAR8, OVCAR4, OVCAR3, and OVSAHO display the hallmark genomic features of HGSC, including widespread gene copy-number alterations, *TP53* mutations, and low frequencies of non-HGSC driver mutations such as *PIK3CA* or *ARID1A*.

Transduction (shRNA human library)

The lentiviral transduction was performed using the MISSION LentiPlex Human TRC 1.0 Pooled shRNA Library (SHPH01) (Sigma-Aldrich, St. Louis, MO). This pooled shRNA library was built on the pLKO lentiviral plasmid backbone (TRC1), which contains the puromycin resistance gene. The library contains approximately 80,000 constructs targeting human genes and is provided in ready-to-use lentiviral particles format at titers of at least 5 x 10^8 TU/ml for efficient gene silencing. The library is pre-divided into 10 subpools, each subpool containing 8,000 clones.

OVCAR8, OVCAR4, and OVCAR3 cells were seeded in 6-well plates, while OVSAHO cells were seeded in 100-mm culture dishes to reach approximately 50% confluency on the day of infection. Cells were incubated overnight at 37 °C in a humidified 5% CO_2 atmosphere. The following day, viral particles from the SHPH01 subpools were thawed at room temperature, kept on ice, and diluted in complete culture medium containing hexadimethrine bromide (polybrene) at a final concentration of 8 µg/mL to enhance transduction efficiency. Each subpool was added separately, resulting in 10 individual transduction samples per cell line. The cells were infected at a multiplicity of infection (MOI) of 1 to ensure that each cell received only a single shRNA construct. After adding the viral mixtures, the plates were gently swirled to distribute the virus evenly, and the cultures were incubated for 18–20 hours under standard conditions. All lentiviral manipulations were carried out under Biosafety Level 2 (BSL-2) containment, adhering to institutional biosafety regulations and good laboratory practices.

After the incubation period, the viral medium was removed and replaced with fresh complete medium without polybrene, allowing the cells to recover for 24 hours. Puromycin selection was then initiated at the predetermined optimal concentration of 1 µg/mL to eliminate non-transduced cells. To monitor the efficiency of the selection, an additional non-transduced control sample was maintained in parallel, enabling us to determine when all non-resistant cells had died. The puromycin-containing medium was refreshed every 2–4 days until only puromycin-resistant cells remained. Once selection was complete, the surviving cell populations were expanded and prepared for downstream

analyses. Genomic DNA from the selected cells was isolated using the DNeasy Blood & Tissue Kit for DNA Isolation (Qiagen, USA).

Genomic DNA concentrations were measured using a NanoDrop spectrophotometer, and sample integrity was verified by agarose gel electrophoresis. The integrated shRNA sequences were then amplified by PCR using primers flanking the hairpin region within the pLKO vector. PCR products of the expected size (approximately 200 bp) were confirmed by agarose gel electrophoresis. All PCR reactions were performed under conditions optimized to preserve the relative abundance of each shRNA, avoiding overcycling.

Barcode library generation and transduction

A high-complexity DNA barcoding library was generated using the Brunello sgRNA backbone coupled to random sequence labels, following the cloning and assembly strategy described by Schmierer et al. (2017) (88). Although the backbone contains CRISPR guide sequences, no Cas9 was expressed in any of the cell lines, ensuring that the constructs functioned solely as neutral DNA barcodes without inducing genome editing.

The final library contained approximately four million unique barcode-guide combinations. Lentiviral particles were produced by transient transfection of HEK293T cells with psPAX2 and pCMV-VSV-G packaging plasmids, and viral supernatants were concentrated using Lenti-X concentrator. The functional titer was determined by puromycin-based survival assays.

All four ovarian cancer cell lines (OVCAR8, OVCAR4, OVCAR3, and OVSAHO) were transduced, and a total of twenty million cells per cell line were infected at a multiplicity of infection of approximately 0.3, generating a pool of roughly six million uniquely barcoded cells. After puromycin selection (2 μg/mL), barcoded populations were expanded to preserve barcode diversity, and approximately one million unique barcodes were implanted per mouse during engrafting.

Xenograft Mouse Model for Ovarian Cancer (Paper V)

The mouse model protocol used for cell implantation and clinical evaluation was based on the protocol and findings of Mitra et al. (2015) (89). The chemotherapy protocol, including the choice of drugs and treatment regimen, was based on Helland et al. (2014) (90).

Animal strain and husbandry

For the in vivo experiments, 6–8 week-old immunocompromised female NOD.Cg-*Prkdc*^{scid} *Il2rg*^{tm1Wjl}/SzJ (NSG) mice were purchased from the Jackson Laboratory (Germany) and housed at the Umeå Centre for Comparative Biology (UCCB). Animals were maintained in individually ventilated cages under controlled environmental conditions, including a regulated temperature and a 12-hour light/dark cycle, and housed in groups of three per cage. Mice were given standard chow and water ad libitum, and cages were equipped with standard enrichment materials to promote natural behavior. Health and welfare were monitored daily by trained UCCB staff, with any abnormal behavior or unexpected morbidity immediately reported to the responsible investigator. All purchased mice were acclimatized at the animal facility for one week prior to the start of the experiment.

Cell implantation

A mixed population of cells from all shRNA subpools, combined in equal proportions, was prepared in vitro. For each mouse, 2×10^6 cells (shRNA experiment) or 5×10^6 cells (barcode experiment) were resuspended in sterile PBS to a final injection volume of 100–200 µL and kept on ice until implantation. To facilitate handling, mice were lightly anesthetized with inhaled isoflurane using a dedicated induction chamber. Cell suspensions were injected into the lower right quadrant of the abdomen, avoiding the urinary bladder, cecum, and other abdominal organs.

Chemotherapy treatment

Ten days after implantation, mice were randomly assigned to two groups: a treatment group (n = 6) receiving carboplatin (15 mg/kg) plus paclitaxel (12 mg/kg), and a control group (n = 6) receiving sterile saline. Both drugs were administered intraperitoneally, at the same occasion but in separate syringes, injected on opposite sides of the abdomen. Treatments were given twice per week for three consecutive weeks.

Tumor monitoring

Tumor development was monitored by palpation and by ultrasound imaging using the Vevo2100 system. Mice were examined closely and weighed weekly to assess general health status and detect early signs of distress or disease progression.

Euthanasia and material collection

Following treatment, animals were monitored for up to three months or until they showed signs of tumor progression or distress requiring humane endpoint

intervention. Mice were euthanized by carbon dioxide inhalation in a dedicated chamber, in accordance with institutional guidelines. After the loss of reflexes, death was confirmed by cervical dislocation. Immediately thereafter, each animal was carefully examined for tumor development and for potential complications such as ascites formation, inflammation of surrounding organs (e.g., pancreatitis), or obstruction of the urinary system. All observations were documented. Tumors and metastatic lesions were collected separately from each organ. Tumor tissues were collected and frozen, and genomic DNA was extracted from a representative portion of each sample for subsequent sequencing analysis.

DNA extraction and PCR amplification

Genomic DNA was extracted from each tumor sample using the DNeasy Blood & Tissue Kit for DNA Isolation, according to the manufacturer's protocol. DNA concentration and purity were initially assessed using a NanoDrop spectrophotometer. The integrated shRNA sequences were then amplified by PCR using primers flanking the hairpin region in the pLKO vector. Multiple parallel PCR reactions were performed per sample to maintain library complexity. PCR products of the expected size (approximately 200 bp) were confirmed by agarose gel electrophoresis and subsequently purified using magnetic beads (ChargeSwitch PCR Clean-Up Kit, Invitrogen). Purified amplicons were quantified using a Qubit fluorometer to ensure accurate concentration measurements for next-generation sequencing. Finally, samples were pooled in equimolar amounts and submitted for high-throughput sequencing to determine the representation of each shRNA within the tumor-derived populations.

shRNA amplification: Genomic DNA from tumor tissues was extracted using the DNeasy blood and tissue kit. The integrated shRNA fragments (~150 bp) were amplified through multiple parallel PCR reactions to maintain representation. PCR forward primer, 5'-CTTGAAAGTATTTCGATTTCTTGGC-3', and reverse primer, 5'-GTGGATGAATACTGCCATTTGTCT-3', were purchased from Integrated DNA Technologies (Heverlee, Belgium). PCR parameters were 95°C for 3 min, followed by 35 cycles at 95°C for 30 s and 62.7°C for 30 s, and final extension at 62.7°C for 5 min. Amplicons were purified by agarose gel electrophoresis and ChargeSwitch magnetic beads (Invitrogen), quantified by Qubit fluorometry, and pooled in equimolar amounts.

Barcode amplification: DNA barcodes were amplified using the PCR strategy described by Schmierer et al. (2017) (88), adapted for the updated primer set used in this study. Multiple parallel reactions were performed per sample to

ensure adequate depth for barcode recovery. Amplicons were purified, quantified, and pooled as described above.

Next-generation sequencing (Paper V)

Library preparation and high-throughput sequencing were performed by Azenta/GENEWIZ (Leipzig, Germany). Amplicon samples were quantified using a Qubit 4.0 fluorometer, and DNA integrity was assessed using an Agilent 5600 Fragment Analyzer. Validated libraries were pooled and loaded onto an Illumina NovaSeq instrument and sequenced using a 2 × 150 bp paired-end configuration. Sequencing was performed to a depth of approximately 10 million read pairs per sample, ensuring sufficient coverage for accurate quantification of shRNA representation.

Barcode libraries were sequenced at SciLifeLab (Stockholm, Sweden) using a custom Read 1 primer for barcode capture, 20 cycles for barcode sequencing, 10 cycles for the i7 index, and 6 cycles for the i5 sample index.

Bioinformatics analysis

shRNA analysis: FASTQ files were processed using the NBIS shRNAseq pipeline. Reads were quality-controlled, adapter-trimmed, and aligned to the SHPH01 reference library. Count tables were generated under three filtering strategies: (1) retaining all shRNAs; (2) excluding shRNAs with zero counts across all samples; and (3) removing shRNAs annotated as off-target. Differential shRNA abundance between groups was assessed with MAGeCK v0.5.9.4. Data quality and reproducibility were evaluated through principal component analysis, hierarchical clustering, shRNA coverage statistics, replicate concordance, and Gini index calculations.

Barcode analysis: Barcode sequences were extracted from raw reads and collapsed into unique barcode identifiers. Barcodes containing unreadable or artefactual sequences (e.g., stretches of poly-G) were removed. Low-abundance noise was minimized by retaining only barcodes with at least ten total reads across all samples. For each sample, barcode abundances were normalized, ranked, and converted into cumulative frequency distributions to quantify clonal representation. Input plasmid libraries were processed in parallel to determine the extent of barcode loss during in vivo tumor establishment.

Statistical Methods

All statistical analyses were performed using IBM SPSS Statistics (version 28 or 29, IBM Corp., Armonk, NY, USA), unless otherwise stated. For the

validation of the LRIG1 Simoa assay, paired comparisons were conducted using a paired Student's t-test in GraphPad Prism, version 5.0 (GraphPad Software, San Diego, CA, USA).

For comparisons between two independent groups, the Mann–Whitney U test was used, and for analyses involving more than two groups, the Kruskal–Wallis test was applied. When multiple comparisons were performed, p-values were adjusted using the Bonferroni correction. Correlations between continuous variables were evaluated using Spearman's rank correlation, while associations between categorical variables were assessed using chi-square tests or Fisher's exact test when expected cell counts were <5. A p-value < 0.05 was considered statistically significant unless otherwise specified.

For comparisons involving clinical characteristics (e.g., histopathological markers, receptor status, or *TP53* and MMR mutation status), chi-square or Fisher's exact tests were applied accordingly. Where appropriate, logistic regression was used to estimate odds ratios (ORs). Logistic regression was chosen because the clinicopathological outcomes of interest were binary or categorical, and this method allows evaluation of how LRIG1 expression (or staining intensity) influences the probability of these clinical endpoints.

Survival Analyses

Survival endpoints included overall survival (OS), cancer-specific survival, relapse-free survival, and disease-free survival (DFS), depending on cohort availability. Survival curves were generated using the Kaplan–Meier method and compared using the log-rank test. Associations between LRIG1 expression and survival outcomes were further assessed with univariable Cox proportional hazards regression, and multivariable Cox models were constructed when sufficient events were available.

For all survival analyses, patients were dichotomized into high- and low-expression groups using either plasma LRIG1 levels or LRIG1 immunohistochemistry (H-score), with the median value used as the cut-off. All results were reported with 95% confidence intervals (CI).

TCGA gene expression survival analyses (Paper IV)

Survival analyses were conducted using molecular and clinical data from the TCGA-UCEC (Uterine Corpus Endometrial Carcinoma) cohort. Molecular profiles and corresponding clinical annotations were obtained from the GDC Data Portal through the TCGAbiolinks R/Bioconductor framework (version 2.34.0). An initial set of 548 cases was retrieved, from which one case lacking definitive survival information was excluded, resulting in 547 samples. The

primary prognostic analysis focused exclusively on the clinically relevant subset of Stage I UCEC cases (n = 341). RNA-sequencing profiles were quantified as Transcripts Per Million (TPM), mapped from ENSEMBL identifiers to official gene symbols, and filtered to retain only protein-coding genes. Overall survival status and OS time (in days) were used as clinical endpoints. Curated and harmonized OS information followed the definitions provided by the TCGA Pan-Cancer Clinical Data Resource (91). After integrating this curated OS information with the processed RNA-seq matrix and restricting the dataset to Stage I tumors, 339 samples contained both complete clinical data and valid expression measurements and were therefore included in downstream analyses.

To define prognostic groups in a data-driven manner, expression thresholds were evaluated across a dense grid of candidate cutoffs spanning the 20th to the 80th percentiles of each gene's expression distribution (TPM). For each candidate threshold, samples were dichotomized into high- and low-expression groups, and group separation was assessed using the log-rank test applied to Kaplan–Meier survival curves. The optimal cutoff for each gene was defined as the expression value yielding the minimum log-rank P-value. All analyses were conducted in the R statistical environment (version 4.4.3).

Ethical considerations

The use of clinical samples and associated data was approved by the relevant ethical review boards, and all patient data were anonymized or pseudonymized prior to analysis. Written informed consent was obtained from all participants or through approved biobank consent procedures.

Cohort #1. The study was performed in accordance with the Declaration of Helsinki and was approved by the ethics committee of the Sahlgrenska University Hospital (Dnr 201-15). All the patients/participants provided written informed consent to participate.

Cohort #2. All procedures were performed in accordance with the Declaration of Helsinki and approved by the Regional Ethical Review Board (Gothenburg, Sweden; case number 767–14). Formalin-fixed paraffin-embedded tumor tissue samples were retrieved from the biobank at Västerbotten County Council with approval from the Regional Ethical Review Board at Umeå University (Dnr 2012-229-31M, 2013-314-32M, and 2022-01127-01).

Cohort #3. The biobanks received ethics approval from their local review boards to collect and share samples and clinical data. All subjects gave broad written consent to future research with their samples and data, without

restriction. Additionally, the central activities of the CRCHUM, which included collection of the COEUR repository samples and data, received local ethics approval by the 'Comité d'éthique de la recherche du Centre hospitalier de l'Université de Montréal (project reference: 2010–3552, CE 09.141 -BSP (CA)).

Cohort #4. Formalin-fixed paraffin-embedded tumor tissue samples were retrieved from the biobank at Västerbotten County Council with approval from the Regional Ethical Review Board at Umeå University (Dnr 2012-229-31M, 2013-314-32M, and 2022-01127-01). Informed consent was obtained at the time of diagnosis, and samples were stored in the biobank for future research. No additional consent was required for this study, as approved by the Ethical Review Board.

In vivo experiments. All procedures were approved by the Regional animal ethics committee (Umeå djurförsöksetiska nämnd, dnr. A2-2020) and were carried out in accordance with institutional and national regulations for the care and use of laboratory animals. Animal experiments were designed in compliance with the principles of Replacement, Reduction, and Refinement (3Rs), with efforts made to minimize animal use and suffering while ensuring scientific validity.

Results and Discussion

PAPER I

Main findings

Development and analytical performance of the LRIG1 Simoa assay

We developed a Simoa assay for detection of LRIG1 in plasma samples using the monoclonal antibodies 3F7 (capture) and 2B7 (detector). The assay demonstrated high specificity, with a 20-fold excess of unlabeled detector antibody blocking 96.5% of the signal. The limit of detection was 1.5 pg/mL, and the dynamic range was 40–2500 pg/mL.

LRIG1 was readily detectable in human plasma. No significant differences were observed between EDTA and citrate plasma (705 ± 225 pg/mL vs. 689 ± 193 pg/mL). LRIG1 levels remained stable after storing whole blood for 4 h at room temperature or 24 h at 4 °C, storing plasma for up to 72 h at room temperature, or subjecting plasma to up to six freeze–thaw cycles. Together, these results showed that the assay was robust to common preanalytical variations.

LRIG1 plasma levels in ovarian tumor patients

LRIG1 plasma concentrations were assessed in 486 patients presenting an ovarian tumor, after exclusion of two extreme outliers. Across the remaining cases, LRIG1 levels progressively increased with degree of malignancy. Mean concentrations were 577 ± 529 pg/mL in benign disease, 645 ± 1222 pg/mL in borderline tumors, 817 ± 800 pg/mL in malignant ovarian cancer, and 857 ± 926 pg/mL in ovary-localized metastases. Statistical analysis confirmed significantly higher LRIG1 levels in malignant compared with benign tumors ($p = 3 \times 10^{-9}$, Bonferroni-adjusted) and borderline tumors ($p = 0.011$). Similarly, LRIG1 levels were elevated in metastases relative to both benign ($p = 8 \times 10^{-5}$) and borderline lesions ($p = 0.026$). A weak but statistically significant positive correlation with age was observed in benign tumors (Spearman's $\rho = 0.224$, $p = 0.005$), whereas no such association was found in borderline or malignant tumors.

When stratified by histotypes, LRIG1 plasma concentrations did not differ significantly among low-grade serous, high-grade serous, mucinous, endometrioid, or clear cell carcinomas ($p = 0.386$, Kruskal–Wallis test). However, LRIG1 levels were significantly higher in advanced-stage disease

(FIGO III–IV) compared with early-stage tumors (FIGO I–II) ($p = 0.003$, Mann–Whitney test).

The apparent response to treatment is strongly dependent on the degree of surgery performed. Radical surgery is associated with a superior response to therapy. Therefore, to evaluate the effect of LRIG1 on the response to chemotherapy, we restricted the analysis to patients who did not receive radical surgery. The median LRIG1 levels were numerically higher in noncomplete responders (1226 pg/mL) compared with complete responders (877 pg/mL). This difference was of borderline significance ($p = 0.051$, Mann–Whitney U test), suggesting that higher levels of plasma LRIG1 might be associated with a worse treatment response.

High LRIG1 plasma levels (above median) were associated with significantly poorer clinical outcomes. In malignant cases, elevated LRIG1 was linked to worse OS ($p = 0.0001$, log-rank test) and shorter DFS ($p = 0.031$). This association remained significant in stage III disease for OS ($p = 0.001$) and DFS ($p = 0.04$). Cancer-specific survival showed no significant association with LRIG1 levels ($p = 0.104$).

Univariable Cox regression identified high LRIG1 as a significant predictor of poor OS in the total malignant cohort (HR = 2.8, 95% CI 1.56–5.00, $p = 0.001$) and in stage III disease (HR = 4.1, 95% CI 1.87–8.78, $p = 0.001$). Additional predictors included CA-125, HE4, age, and nonradical surgery. In type I, stage III tumors, LRIG1 was the only significant prognostic factor ($p = 0.01$), whereas in type II, stage III tumors, both LRIG1 ($p = 0.02$) and nonradical surgery ($p \leq 0.001$) were associated with survival.

In multivariable Cox models, HE4 ($p = 0.027$), age ($p = 0.006$), and nonradical surgery ($p \leq 0.001$) remained independently associated with OS in the malignant cohort. In stage III disease, LRIG1 ($p = 0.002$), age ($p = 0.046$), and nonradical surgery ($p < 0.001$) were retained as independent prognostic markers. In contrast, within type II, stage III tumors, only nonradical surgery remained significant ($p = 2.3 \times 10^{-5}$).

Discussion

When validating the LRIG1 Simoa assay, the mean LRIG1 concentration in healthy donors (705 pg/mL) was substantially higher than a previous mass-spectrometry-based estimate (78 pg/mL), consistent with known discrepancies between immunoassays and spectral-counting–based quantification. Potential explanations include limited accuracy of spectral counting and the possibility

that alternative LRIG1 forms lacking antibody epitopes may exist. Thus, while the absolute levels remain uncertain, the assay was highly suitable for sensitive and reproducible measurement of LRIG1 in biological fluids.

In our study, lower plasma LRIG1 protein levels were associated with better survival in ovarian carcinoma, contrasting with the findings of Willis et al. (2011), who reported that low LRIG1 tumor mRNA expression predicted poor survival in ovarian serous carcinoma. Several factors may account for this discrepancy. Willis et al. measured LRIG1 mRNA in tumor tissue, whereas we quantified circulating LRIG1 protein, and mRNA–protein correlations are often weak. Moreover, it is unclear whether elevated plasma LRIG1 reflects increased levels of functional LRIG1 in the tumor or, alternatively, proteolytic shedding and inactivation of cellular LRIG1. Supporting this complexity, the TCGA ovarian cancer dataset **(**(http://www.tsvdb.com/plot.html) includes a common LRIG1 transcript variant (isoform_uc011bfu) that lacks the 5′ region encoding the leucine-rich repeats and may therefore produce a nonfunctional protein. Finally, circulating LRIG1 may originate from non-tumor tissues, although such sources have not yet been identified. To resolve these inconsistencies, future studies should measure plasma LRIG1 protein and tumor LRIG1 mRNA in the same patients and determine the cellular origin of circulating LRIG1.

High plasma LRIG1 was consistently associated with more advanced disease, poorer treatment response, and worse OS in ovarian carcinoma. Notably, in type I, stage III tumors, LRIG1 outperformed CA-125, HE4, age, and the extent of cytoreductive surgery as the sole significant predictor of survival. These findings contrast with previous reports describing LRIG1 as a tumor suppressor (64, 67, 82, 92, 93, 94), but may be explained by its recently identified role as a promoter of BMP signaling (71). While BMP signaling suppresses many tumor types, it appears to enhance growth and correlate with poor prognosis in ovarian carcinoma, suggesting that LRIG1 may act as a tumor promoter in this context (95-98). From a clinical perspective, if validated, LRIG1 could support risk assessment by identifying patients with particularly aggressive disease who might benefit from more intensive treatment strategies. However, before LRIG1 can be implemented as a predictive biomarker, it will be essential to determine whether elevated LRIG1 levels are associated not only with poor prognosis but also with differential response to specific therapies, particularly chemotherapy. Future studies should therefore investigate whether LRIG1 expression can inform treatment decision-making or guide personalized therapeutic approaches.

PAPER II

Main findings

High LRIG1 expression predicts lymph node metastasis in patients with uterine cervical cancer

Sixty-seven patients with uterine cervical cancer who underwent Wertheim–Meigs surgery at Umeå University Hospital between 1997 and 2021 were included in the analysis. Baseline characteristics such as age and body mass index did not differ significantly between patients with lymph node metastasis (LN-positive) and those without (LN-negative). Smoking was more frequent among LN-positive patients (29% vs. 10%), although this difference did not reach statistical significance ($p = 0.062$). All patients were restaged according to FIGO 2018; only early-stage disease was identified preoperatively, and patients with lymph node involvement were reclassified as stage IIIC postoperatively. The majority of tumors were classified as squamous cell carcinoma (61%) or adenocarcinoma (34%). Adjuvant treatment consisted of radiotherapy in 47 patients and chemotherapy in 28 patients.

During five years of follow-up, eight patients died, seven of whom were in the LN-positive group. Disease recurrence occurred significantly more often among LN-positive patients compared with LN-negative patients (33% vs. 7%, $p = 0.009$), consistent with the established prognostic impact of lymph node metastasis in cervical cancer (99-102).

p16 immunostaining was successful in all tumors, with 94% testing positive, reflecting HPV-driven oncogenesis, and no difference in p16 status was observed between LN-positive and LN-negative groups ($p = 0.379$) (103-105). LRIG1 staining was unsuccessful in five cases. Among the remaining tumors, LRIG1 immunoreactivity was predominantly nuclear. Seventeen tumors (27%) showed no detectable LRIG1 expression, whereas only two cases (3%) demonstrated expression in more than 75% of tumor cells. Staining intensity was generally weak to low.

LRIG1 expression differed significantly between LN-positive and LN-negative patients ($p = 0.011$). When patients were dichotomized according to LRIG1 expression levels, using a cutoff of >25% positive tumor cells, high LRIG1 expression was strongly associated with lymph node metastasis ($p < 0.001$). This association remained statistically significant in both univariable (OR = 8.47, 95% CI 2.15–33.37, $p = 0.002$) and multivariable logistic regression analyses (OR = 9.49, 95% CI 1.80–50.05, $p = 0.008$). In contrast, LRIG1

staining intensity alone was not associated with LN status ($p = 0.320$), and no relationship was found between LRIG1 expression and p16 positivity.

Discussion

Earlier reports have described high LRIG1 expression as a favorable prognostic marker in early-stage squamous cell carcinoma (76) and adenocarcinoma (77). In contrast, our findings suggest that LRIG1 may also be relevant as a predictor of lymph node metastasis (LNM). We observed significantly higher LRIG1 expression in LN-positive compared with LN-negative patients. Although this may appear contradictory, it is important to emphasize that these studies addressed different endpoints. While previous investigations evaluated LRIG1 in relation to overall prognosis, our study focused specifically on its ability to predict lymphatic spread. Similar context-dependent findings have been reported in non-small-cell lung cancer, where high LRIG1 expression was associated both with improved survival (81) and with mediastinal lymph node metastasis (106). These discrepancies may partially be explained by the biological significance of LRIG1 subcellular localization. In our study, LRIG1 immunoreactivity was predominantly nuclear, a pattern also observed in several other malignancies, including basal cell carcinoma (107), non-small-cell lung cancer (81), and head and neck cancer (80). Moreover, shifts in subcellular localization appear to occur with disease progression; for example, LRIG1 transitions from primarily nuclear in normal skin to cytoplasmic in psoriatic lesions (108). These observations suggest that the clinical and prognostic implications of LRIG1 depend on the biological context, cellular localization, and stage of the disease.

Strengths of this study include a well-characterized cohort and detailed clinical annotation. Limitations include the retrospective design, relatively small sample size, and single-center setting. The use of a polyclonal LRIG1 antibody may also limit reproducibility; future studies should evaluate standardized monoclonal antibodies. Also, because cervical cancer is easily accessible for biopsy, LRIG1 immunostaining could potentially be used preoperatively to predict LNM and guide treatment decisions. Larger independent cohorts will be needed to validate LRIG1 as a clinically meaningful biomarker. Recent developments in measuring LRIG1 in plasma (109) suggest that blood-based testing may also offer a promising, less invasive alternative for future evaluation.

Our results suggest that LRIG1 expression may serve as a potential biomarker for predicting lymph node metastasis in cervical cancer and warrants further investigation. From a clinical perspective, identifying patients at risk of LNM

before surgery is highly relevant, as those with suspected nodal involvement may be treated with primary chemoradiotherapy, which provides similar oncological outcomes to surgery. However, when surgery is performed and LNM is detected only postoperatively, adjuvant chemoradiotherapy must be added, resulting in comparable survival but considerably higher treatment-related morbidity. Therefore, if LRIG1 expression could be assessed preoperatively it may help refine treatment selection and reduce unnecessary toxicity.

To implement LRIG1 as a clinically actionable biomarker, several steps are required. The current study used a polyclonal antibody in a relatively small cohort, which may limit reproducibility. Future validation using standardized monoclonal antibody–based assays is needed, along with larger retrospective and prospective studies to determine whether LRIG1, alone or in combination with other markers, can reliably predict LNM in early-stage cervical cancer. Additionally, a recently developed plasma-based LRIG1 detection method (109) offers a less invasive alternative that could be further explored for biomarker purposes.

PAPER III

Main findings

Development and validation of the monoclonal anti-LRIG1 antibody

To enable consistent and long-term assessment of LRIG1 expression in tumor tissues, we developed a monoclonal antibody (clone 10C8) targeting the same cytosolic LRIG1 peptide previously used for generating the polyclonal antibodies LRIG1-151 and LRIG1-Vina (110). In total, approximately 2,000 hybridoma colonies were screened by ELISA, of which 19 showed positive reactivity. Only one clone, 10C8, was additionally reactive in Western blotting and was therefore selected for further development. Optimization using formalin-fixed paraffin-embedded LRIG1-null and LRIG1-expressing HEK293T cell pellets demonstrated that a concentration of 1 µg/mL yielded the optimal signal-to-noise ratio in immunohistochemistry. Using this optimized protocol, 10C8 produced highly specific staining patterns, with generally weak LRIG1 immunoreactivity in ovarian carcinoma tissues. This finding is consistent with data from the Human Protein Atlas, where LRIG1 staining in normal and neoplastic ovarian tissues is also described as relatively weak (111, 112).

LRIG1 immunoreactivity in ovarian carcinoma cohorts

LRIG1 tumor immunoreactivity was evaluated by immunohistochemistry across three independent ovarian carcinoma cohorts, comprising a total of 761 patients. Cohort #1 comprised 430 patients with suspected pelvic masses, in which 123 patients had benign diseases of the ovary, 70 had borderline-type tumors, 213 had malignant ovarian tumors, and 29 had ovary-localized metastases. Cohort #2 (n = 205) consisted of early-stage (FIGO I–II) ovarian carcinomas, including 94 high-grade serous (HGSC), 46 endometrioid, 37 clear cell, and 28 mucinous carcinomas. Cohort #3 (n = 70) comprised LGSC cases collected as part of the COEUR biobank.

In Cohort #1, previously measured plasma LRIG1 levels (Simoa assay) were compared with tumor H-scores. Among patients with type II tumors, we identified a statistically significant inverse correlation between tumor LRIG1 immunoreactivity and plasma protein levels (Spearman's $\rho = -0.175$, $p = 0.042$). No significant associations were detected in type I tumors, benign cases, borderline lesions, or metastatic tumors ($p > 0.05$). In Cohort #2, LRIG1 transcript levels were available for 95 tumors (RNA-seq). A weak but statistically significant positive correlation was observed between LRIG1 H-scores and LRIG1 mRNA expression (Spearman's $\rho = 0.259$, 95% CI 0.055–

0.443, $p = 0.011$, $R^2 = 0.031$), indicating that higher transcript levels were associated with increased protein immunoreactivity.

In Cohort #1, LRIG1 immunoreactivity differed significantly across malignancy categories (Kruskal–Wallis, $p < 0.001$). Malignant tumors exhibited higher H-scores than benign lesions ($p < 0.001$) and metastatic tumors ($p = 0.009$, Bonferroni-adjusted). A non-significant trend toward increased LRIG1 expression was observed in malignant compared with borderline tumors ($p = 0.084$). No significant differences were found among benign, borderline, and metastatic groups ($p > 0.05$).

Histotype stratification in Cohort #1 showed no significant variation among benign tumors ($p = 0.068$). However, in borderline tumors, LRIG1 H-scores varied significantly (Kruskal–Wallis, $p = 0.011$), with serous tumors displaying higher expression than mucinous tumors (adjusted $p = 0.008$). Among malignant tumors, no statistically significant differences were detected between histotypes ($p = 0.149$), although serous carcinomas tended to exhibit higher LRIG1 expression than mucinous carcinomas.

In Cohort #2, significant variation in LRIG1 expression was observed across histotypes at both the protein (H-score: $p < 0.001$) and transcript levels (mRNA: $p = 0.018$). Median LRIG1 expression was highest in HGSC and lowest in clear cell carcinoma, with endometrioid and mucinous tumors demonstrating intermediate levels.

Prognostic implications of LRIG1 immunoreactivity

One of the motives behind this study was our previous finding that LRIG1 plasma levels were increased in ovarian carcinoma patients and that this was a prognostic marker in both type I and type II disease (109). In Cohort #1 ($n = 208$ malignant ovarian tumors), LRIG1 immunoreactivity was evaluated in relation to OS, cancer-specific survival (CSS), and DFS, with analyses stratified by the dualistic model (type I vs. type II tumors) and merged FIGO stages (I/II vs. III/IV). Surprisingly, among type II patients, we found that LRIG1 immunoreactivity did not correlate with survival.

Among patients with advanced-stage type I tumors (FIGO III/IV), higher LRIG1 H-scores were significantly associated with improved CSS (log-rank $p = 0.021$). This was supported by univariate Cox regression, where elevated LRIG1 expression (log-transformed) was associated with a reduced risk of cancer-specific death (HR = 0.016, 95% CI 0.000–0.932; $p = 0.046$). In contrast, in early-stage type I tumors (FIGO I/II), higher LRIG1 expression showed a non-significant trend toward reduced CSS ($p = 0.053$), suggesting a

stage-dependent prognostic effect. In LGSC patients from Cohort #1 (n=22), LRIG1 expression demonstrated a strong association with DFS (log-rank test, $p = 0.009$). In fact, there was only one recorded disease recurrence among the patients with high LRIG1 expression (n = 10), while 7 of 12 patients (58.34%) with low expression experienced disease progression.

To further investigate the association between LRIG1 immunoreactivity and LGSC patient survival, we analyzed a larger LGSC cohort, Cohort #3, comprising 70 LGSC cases. However, no significant association was observed between LRIG1 expression and OS ($p = 0.347$), CSS ($p = 0.440$), or DFS ($p = 0.215$), and LRIG1 was not prognostic in multivariable Cox analysis. In Cohort #3, LRIG1 immunoreactivity was additionally assessed in relation to postoperative residual disease. Higher LRIG1 H-scores correlated with larger residual tumor burden (Spearman's $\rho = 0.294$, $p = 0.040$). Consistently, patients with macroscopic residual disease > 1 cm or miliary spread (n = 20) displayed higher LRIG1 expression compared to those with none or ≤ 1 cm residual disease (n = 29; mean rank 29.65 vs. 21.79; Mann–Whitney $p = 0.042$). No significant associations were observed with age ($p = 0.089$), tumor grade ($p = 0.904$), or FIGO stage ($p = 0.208$).

Discussion

Monoclonal and polyclonal antibodies differ in their origin, specificity, and binding characteristics. Polyclonal antibodies are produced by multiple B-cell clones and thus recognize several epitopes on the same antigen, which can enhance detection sensitivity but may also increase nonspecific background staining or cross-reactivity. In contrast, monoclonal antibodies are derived from a single B-cell clone and bind to a single, well-defined epitope, providing superior specificity, batch-to-batch consistency, and reproducibility. These properties make monoclonal antibodies particularly advantageous for immunohistochemistry, where precise and uniform antigen recognition is essential for reliable interpretation.

The successful validation of 10C8 therefore represents an important methodological advance, providing a reproducible and standardized immunoreagent for LRIG1 assessment. By eliminating variability associated with polyclonal reagents, this antibody will enable more comparable and reliable immunohistochemical studies going forward, supporting the investigation of LRIG1's role in ovarian carcinoma and other tumor types.

This is, to our knowledge, the first thorough investigation of LRIG1 immunoreactivity in ovarian carcinoma. With the new antibody, we analyzed

LRIG1 tumor immunoreactivity in three different ovarian carcinoma cohorts, comprising 761 patients, in total. The staining pattern obtained with the 10C8 antibody was highly specific, with overall weak immunoreactivity in ovarian carcinoma tissues. This agrees with data from the Human Protein Atlas, where LRIG1 staining in normal and neoplastic ovarian tissues are also described as relatively weak (111, 112). Taken together, these results indicate that LRIG1 expression increases with malignant transformation and varies across ovarian cancer histotypes, particularly in HGSC. This histotype-specific expression pattern aligns with established molecular distinctions between tumor subtypes and suggests that LRIG1 may be linked to underlying biological characteristics of ovarian carcinoma.

Here, we were also able to evaluate LRIG1 tumor protein expression by immunohistochemistry in the same patient cohort, i.e., in Cohort #1. In the type 2 tumors (HGSC), there was an inverse correlation between LRIG1 tumor immunoreactivity and LRIG1 plasma levels. Currently, we do not know the reason for this apparent contradiction. One speculation, however, could be that plasma LRIG1 represents (proteolytically) shed LRIG1, and that increased shedding activity results in the concomitant increase of plasma LRIG1 and decrease of tumor cell LRIG1 expression by reducing membrane-bound or cellular LRIG1. Indeed, it is known that LRIG1 can be cleaved and shed from cells by the metalloprotease ADAM17 (113). If so, the levels of LRIG1 in plasma and tumor cells would be reciprocally regulated by the sheddase activity. This could then also explain the relatively poor, although significant, correlation between LRIG1 tumor immunoreactivity and LRIG1 transcript levels.

The contrasting prognostic results in LGSC patients obtained from Cohort #1 and Cohort #3 may reflect differences in clinical characteristics from both cohorts (e.g., stage distribution, treatment strategies, and follow-up duration) and suggest that LRIG1 may only be prognostically relevant in specific LGSC subgroups. To resolve the possibility that LRIG1 tumor immunoreactivity might be a strong prognostic factor in a specific subgroup of LGSC, further investigations are needed.

In Cohort #3, the observed association between LRIG1 expression and residual disease was derived from exploratory analyses and, therefore, requires validation. Nevertheless, it suggests that LRIG1 expression may be related to tumor persistence or surgical resectability in LGSC. Nevertheless, if true, it suggests, together with the possible associations between LGSC patient survival and LRIG1 tumor immunoreactivity and plasma levels, that LRIG1 could play an etiological role in the development of LGSC. LGSC is characterized by frequent *KRAS* and *BRAF* mutations (114) and activation of the

RAS/RAF/MEK/MAPK pathway (115), which LRIG1 has been shown to modulate in various contexts (62, 63, 67, 116). However, further mechanistic and molecularly stratified studies are required to determine whether LRIG1 plays an etiological role in LGSC or acts as a surrogate marker of underlying tumor biology.

In summary, in Paper III, we developed and validated a new LRIG1 antibody for immunohistochemistry and used it to analyze 761 ovarian carcinoma cases. This revealed histotype-specific staining patterns, an intriguing reverse association between tumor immunoreactivity and plasma protein levels, and a possible role for LRIG1 as a prognostic factor in LGSC. Further studies are needed to elucidate the mechanisms underlying the reciprocal regulation of LRIG1 tumor immunoreactivity and LRIG1 plasma levels as well as the possible roles of LRIG1 as a prognostic marker and an etiological factor in LGSC.

PAPER IV

Main findings

BMP signaling regulators and survival in stage I endometrioid endometrial carcinoma

We assessed the prognostic value of BMP signal regulators using transcriptomic data from 339 FIGO stage I endometrioid endometrial carcinomas from the TCGA Uterine Corpus Endometrial Carcinoma cohort available via the GDC Data Portal. Transcript levels of 34 established BMP pathway regulators, including ligands, receptors, co-receptors, antagonists, SMAD proteins, and importins (117, 118), were analyzed. Of the 34 BMP signal regulator genes analyzed, nineteen were significantly associated with patient survival. Poor survival was associated with high levels of five ligands, two receptors, two co-receptors or promoters, one antagonist, four Smad proteins, and three importins. Good survival was associated with high levels of one receptor and one antagonist. Taken together, most of the directions of the associations between BMP signal regulator genes and patient survival (16/19) suggested that enhanced BMP signaling was bad for survival among the endometrioid endometrial carcinoma stage I patients.

LRIG1 protein expression and prognosis in stage I endometrioid endometrial carcinoma

To evaluate candidate biomarkers identified in the transcriptomic analysis, we constructed a tissue microarray of 241 FIGO stage I endometrioid endometrial carcinomas. The median patient age was 65 years (range 37–88). Most tumors were stage IA (76.8%) and well or moderately differentiated (92.5%). All patients underwent hysterectomy with bilateral salpingo-oophorectomy; 22.9% received adjuvant external radiotherapy, 15.4% brachytherapy, and 6.6% chemotherapy. Over a median follow-up of nine years, 19 patients (7.9%) experienced recurrence (local recurrence: n = 8, distant metastasis: n = 6, both: n = 4), consistent with the expected favorable prognosis of early-stage disease.

In this study, we restricted the immunohistochemical analysis of prognostic candidate markers to the BMP signal promoter LRIG1, selected due to the availability of a validated monoclonal antibody. The immunohistochemical LRIG1 analysis revealed that the cases were rather evenly distributed across the four categories of combined LRIG1 score, indicating a suitable dynamic range. Seventy-one samples (29.5%) were completely devoid of LRIG1 immunoreactivity (combined LRIG1 score 0), 68 samples (28.2%) showed weak staining in the minority of cells (combined LRIG1 score 2), 66 samples

(27.4%) showed weak staining in the majority of cells or strong staining in the minority of cells (combined LRIG1 score 3), and 36 samples (14.9%) showed intense staining in the majority of tumor cells (combined LRIG1 score 4).

Univariable Cox analysis identified age, histological grade, and lymphovascular space invasion (LVSI) as significant prognostic factors. In multivariable analysis, only grade (HR 3.9, $p = 0.02$) and LVSI (HR 12.3, $p < 0.001$) remained independent predictors; age over 64.5 years showed borderline significance ($p = 0.05$). LRIG1 immunoreactivity was not prognostic in either model. Kaplan–Meier analysis confirmed no association between LRIG1 score and relapse-free survival ($p = 0.70$). Although LRIG1-strong tumors had numerically fewer recurrences (5.7% compared with 11.8% in LRIG1-negative cases), the difference was not significant ($p = 0.33$). Analysis of staining intensity or cell positivity did not improve prognostic value. These results contrast with TCGA transcriptomic data, where high LRIG1 expression showed a trend toward poorer outcome ($p = 0.063$).

Lastly, LRIG1 expression correlated significantly with ER ($p = 0.006$), PR ($p = 0.025$), and Ki-67 ($p = 0.002$), consistent with known estrogen-dependent regulation of LRIG1 (119). No significant associations were detected with *TP53* or MMR status, differentiation grade, FIGO stage, or LVSI, although a borderline trend toward higher LRIG1 expression in *TP53*-mutated cases was observed ($p = 0.051$). Analysis by molecular subgroup, however, could not be performed due to missing *POLE* mutation data. Future studies should evaluate LRIG1 in defined molecular groups and explore additional BMP pathway regulators at the protein level.

Discussion

Here, we showed that the expression levels of 19 BMP signal-regulating genes were of prognostic significance in endometrioid endometrial carcinoma stage I. Intriguingly, the expression of the vast majority of BMP signal-promoting genes was associated with worse survival, whereas expression of the signal-antagonistic Noggin gene was associated with good survival. This suggests that BMP signaling as such might be a risk factor in early-stage endometrioid endometrial carcinoma. Although the role of BMP signaling in endometrioid endometrial carcinoma is not completely understood, our results align with the report by Fukuda et al., which suggested that BMP signaling promoted endometrial cancer (96). Therefore, it will be interesting to investigate if a biochemical readout of BMP signaling, such as the detection of phosphorylated SMAD1/5, can serve to identify early-stage endometrioid endometrial

carcinoma patients with an increased risk of relapse in a clinically meaningful manner.

Future studies should investigate whether biochemical markers of BMP activity, such as phosphorylated SMAD1/5, or immunohistochemical profiling of BMP regulatory proteins (e.g., LRIG1, LRIG3), alone or in combination, can improve prognostic assessment and support risk stratification in early-stage endometrioid endometrial carcinoma. Such approaches may also help identify patients most likely to benefit from treatment targeting BMP-associated mechanisms.

The prognostic value of LRIG1 immunoreactivity in endometrioid endometrial carcinoma was also investigated by Razumova et al. (2021), who reported no prognostic relevance of LRIG1 protein expression in their cohort (120). In that study, LRIG3, rather than LRIG1, emerged as prognostically relevant and was more highly expressed in type I tumors. However, in this study, the LRIG1 antibody used was poorly characterized, and 50 out of 51 type I carcinomas received the highest LRIG1 staining score which is in strong contrast to the more modest LRIG1 stainings of endometrial carcinomas observed in other studies, such as is seen in the human protein atlas. Negative controls were also not reported in the study. The use of a validated monoclonal antibody in our study likely enabled a more accurate assessment of LRIG1.

In the tissue microarray cohort, the prognostic values of patient age, histological grade and LVSI status were confirmed in univariable analyses but only patient age and LVSI status were significant independent prognostic markers in the multivariable analysis. Endometrial carcinoma is generally associated with a good prognosis, especially if diagnosed at an early stage, which most often is the case. This favorable prognosis was confirmed in our study, with more than 90% of patients showing no signs of relapse during the follow-up period. With few events of relapse, it is expected that prognostic markers with weak or moderate levels of influence would require a larger sample size to show significant correlations. The tumor characteristic that was by far the strongest prognostic indicator in the tissue microarray cohort was the presence of LVSI with a hazard ratio of 9.0 in a univariable analysis and 9.5 in a multivariable analysis, substantially higher than those typically reported in early-stage disease (commonly 1.8–3.4). This may be explained by reduced inter-observer variability, since all histopathological assessments were carried out by a single subspecialized gynecologic pathologist.

In summary, although several BMP-associated transcripts were linked to recurrence risk in stage I endometrioid endometrial carcinoma, LRIG1 protein expression did not show prognostic value. The tissue microarray developed in

this study provides a valuable resource for future research into BMP-regulating proteins as potential immunohistochemical biomarkers in early-stage disease.

PAPER V

Main findings

Tumour formation across four human ovarian cancer cell lines

In this study, we implanted four different human ovarian carcinoma cell lines, OVCAR3, OVCAR4, OVCAR8, and OVSAHO, into the peritoneal cavity of immunocompromised NSG mice. Before implantation, the cells were barcoded through the transduction of the cells with either an shRNA library containing 81,816 different shRNAs or a gRNA library containing approximately 1 million barcodes. In the first experimental series, 2 million shRNA-transduced cells were implanted and in the second experimental series, 5 million gRNA-transduced cells were implanted into each mouse. In all experiments, all four cell lines successfully formed intraperitoneal tumors in all the implanted mice. Tumor development occurred at variable rates across cell lines but was consistently detectable by ultrasound imaging within two to three weeks, although ultrasound imaging was used only in the first experimental series. Notably, all cell lines formed tumors at sites typical for high-grade serous ovarian carcinoma such as in the ovaries, mesentery, liver, pancreas, peritoneal wall, and diaphragm. Approximately half of the mice transplanted with OVCAR3 and OVCAR8 also showed small white tumors floating in the associated ascites. Overall, we found the metastatic patterns for all four cell lines fairly similar to the patterns seen for human high-grade serous ovarian carcinoma, which also frequently included carcinomatosis.

Effects of chemotherapy

In experiment 1, mice were treated either with chemotherapy, comprising a combination of carboplatin and paclitaxel, or with saline, as control, twice a week for three-to-four weeks. When one or a few mice lost weight or showed signs of sickness, the whole corresponding experimental group was sacrificed and necropsied. Chemotherapy-treated animals generally developed smaller and fewer macroscopic tumors than the control mice, consistent with partial sensitivity to the carboplatin–paclitaxel combination therapy in vivo. Notably, while treatment reduced overall tumor burden in all four xenograft models, it did not completely eradicate the cancer in any of the treated mice.

Frequency of tumor-initiating cells in the xenograft models

To determine the frequency of tumor-initiating cells in the xenograft models, we performed two barcode experiments. In the first experiment, cell lines were retrovirally transduced with an shRNA library comprising 81,816 different shRNA sequences. However, upon NGS, only approximately 7,000–14,000

shRNAs were detected in the transduced cell lines (e.g., 6,613–8,701 in OVCAR3; 7,073–9,283 in OVCAR4; 7,424–8,186 in OVCAR8; and 10,569–13,926 in OVSAHO). We do not know why only 8–17% of the original library was represented in the cell populations after transduction and puromycin selection. Nevertheless, we used the transduced shRNA sequences as cellular barcodes in the analyzed tumors. The mice were either treated or not treated with chemotherapy, and thereafter the tumors were harvested and subjected to NGS to determine the representation of the different shRNA sequences in the tumors. In the saline-treated control mice, between 552 and 2,717 shRNAs (OVCAR4 and OVCAR8, respectively) were detected in each mouse. Because 2 million cells were implanted in each mouse, these numbers suggest that only approximately 3-to-10 of 10,000 implanted cancer cells contributed to tumor formation in the control mice. In the chemotherapy-treated mice, the number of detected shRNAs were, in general, lower, corresponding to 1.5×10^{-4} - 4.7×10^{-4} tumor-initiating cells, which first formed tumors and then also survived the chemotherapy.

In the second barcode experiment, OVCAR3 and OVCAR8 were retrovirally transduced with a DNA barcode library comprising approximately one million unique barcodes. Approximately 6-to-8 weeks after implantation, tumors were harvested and analyzed. Between 650 and 1,000 barcodes could be detected in each mouse, and the tumors tended to be more than 90% made up of 250-500 barcodes, corresponding to unique cell lineages. Because here, 5 million cells were implanted in each mouse, the number of identified barcodes suggests that approximately $1.5 – 2 \times 10^{-4}$ of the implanted cancer cells contributed to tumor formation in each mouse, which was very similar to the results of the control mice in the shRNA experiment described above ($3 – 10 \times 10^{-4}$ cells).

Discussion

The shRNA library approach enables systematic loss-of-function (LOF) screening of many genes simultaneously. Each shRNA construct expresses a short RNA sequence designed to form a hairpin structure that is processed by the cellular RNA interference (RNAi) machinery into a small interfering RNA (siRNA). This siRNA binds to the complementary messenger RNA (mRNA) of the target gene, leading to its degradation or translational repression, resulting in stable gene knockdown.

When a pooled shRNA library is introduced into a population of cells, each cell receives a different shRNA, effectively silencing a different gene. Over time, comparing the representation of each shRNA in the population before and after selection (e.g., drug treatment or tumor formation) allows identification of

genes that are essential for cell survival, proliferation, or therapeutic resistance. Enrichment of certain shRNAs indicates silencing of tumor-suppressor genes, while depletion ("dropout") of others suggests targeting of essential or oncogenic genes. This approach, described in detail by Gargiulo et al. (2014), has become a powerful tool for discovering new cancer-related genes and for understanding gene function in complex biological contexts (121).

In this study, we evaluated four different ovarian carcinoma human-mouse xenograft models with regard to their transplantation-ability, disease time course, metastatic pattern, chemosensitivity, and frequency of tumor-initiating cells. All four tested human ovarian carcinoma cell lines were tumorigenic in NSG mice and they were sensitive to a clinical-like chemotherapy regimen, including carboplatin and paclitaxel. However, the rather low proportion of tumor-initiating cells will impose important limitations on the planned genetic screens aiming to elucidate the genetic determinants of treatment resistance in high-grade serous ovarian carcinoma.

The ultimate goal of this project is to perform genetic screens in vivo to elucidate the genetic determinants of treatment resistance in high-grade serous ovarian carcinoma. To this end, a representative experimental system will be instrumental to be able to obtain knowledge that is translatable to the human clinical situation. Here, we chose to investigate a series of xenograft models that were based on established human ovarian carcinoma cell lines, namely the OVCAR3, OVCAR4, OVCAR8, and OVSAHO cell lines. These cell lines were chosen because of their genomic and transcriptomic similarities to human high-grade serous ovarian carcinoma as manifested in the TCGA database (24). Other important criteria in our selection of cell lines were their availability and tumorigenicity in immunocompromised mice. Hence, all the analyzed cell lines were previously shown to be tumorigenic in immunocompromised nude mice, whereas, for example, the cell line ranked most similar to high-grade serous ovarian carcinoma by Domcke et al. (24), Kuramochi, was not (89). Overall, our results confirmed that all the tested cell lines were highly tumorigenic after intraperitoneal implantation into NSG mice, with an observed take rate of 100%. Furthermore, and importantly, they showed human-like morphologies and anatomical metastatic patterns Therefore, we believe that all four xenograft models tested, represent potentially relevant in vivo models of human high-grade serous ovarian carcinoma.

We also wanted to incorporate a clinically relevant chemotherapy regimen into the model. Specifically, we included the widely used carboplatin – paclitaxel combination therapy paradigm. To this end, we adapted the optimized treatment protocol developed by Helland et al. (90). This included bi-weekly intraperitoneal injections of the drug combination for 3-to-4 weeks. In all four

xenograft models, this treatment resulted in reduced tumor growth, although not complete tumor eradication. This resembles the human situation and is therefore an important feature of the models.

The frequency of tumor-initiating cells was in all models between 1 x 10^{-4} and 10 x 10^{-4}. This result will guide future genetic screens in the analyzed xenograft models. In our current ethical permit, we are restricted to a maximal intraperitoneal injection volume of 0.5 milliliter. It will, therefore, be difficult to implant more than 5 million cells per mouse, corresponding to between 500 and 5,000 tumor-initiating cells. Hence, it will not be realistic to screen more than approximately 150 genes per mouse in this experimental setting.

In summary, all four xenograft models, comprising the human ovarian carcinoma cell lines OVCAR3, OVCAR4, OVCAR8, and OVSAHO and NSG mice, were found to recapitulate important features of human high-grade serous ovarian carcinoma. These features included human-like metastatic patterns and partial sensitivity to carboplatin and paclitaxel combination therapy. Given the relatively low frequency of tumor-initiating cells in the injected cell populations, future genetic screens have to be designed accordingly.

Conclusions

The overall aim of this thesis was to explore the potential role of LRIG1 as a biomarker in gynecological cancers, focusing on its prognostic value and association with clinically relevant features, and to develop a translatable in vivo model for the genetic screening of drug targets in high-grade serous ovarian carcinoma.

To achieve this, we:

- Developed and validated a method to measure LRIG1 in plasma, demonstrating prognostic relevance in ovarian cancer.
- Generated a monoclonal LRIG1 antibody (10C8) suitable for immunohistochemistry and applied it to several patient cohorts.
- Assessed the prognostic significance of LRIG1 tumor expression, identifying significant associations in advanced-stage type I ovarian cancer and cervical cancer with lymph node metastasis.
- Established a xenograft mouse model for ovarian cancer, supporting future functional studies.
- Evaluated pooled genomic screening feasibility in an intraperitoneal setting, identifying both opportunities and biological limitations.

Together, these findings provide new insights into the clinical and biological relevance of LRIG1 in gynecological cancers and form a basis for further mechanistic and validation studies.

References

1. Zhu X, Chen W, Liu H, et al. Global Burden of Gynaecological Cancers in 2022 and Projections to 2050. Lancet Glob Health. 2024.
2. Mazidimoradi A, Salehiniya H, Almasi Z, et al. The Global Incidence, Mortality, and Burden of Uterine Cancer: Trends and Projections to 2050. BMC Public Health. 2024;24:1452. https://pubmed.ncbi.nlm.nih.gov/38274134
3. International Agency for Research on Cancer (IARC). Cervical Cancer Fact Sheet. IARC, World Health Organization, 2023. https://www.iarc.who.int/cancer-type/cervical-cancer
4. Bruni L, Diaz M, Barrionuevo-Rosas L, et al. Global estimates of human papillomavirus vaccination coverage by region and income level: a pooled analysis. Lancet Glob Health. 2016;4(7):e453-e463. doi:10.1016/S2214-109X(16)30099-7
5. Singh D, Vignat J, Islami F, et al. Global Estimates of Incidence and Mortality of Cervical Cancer in 2020: A Systematic Analysis. BMC Cancer. 2022;22:1096.
6. Bowtell, D. D., Böhm, S., Ahmed, A. A., Aspuria, P. J., Bast, R. C., Jr, Beral, V., Berek, J. S., Birrer, M. J., Blagden, S., Bookman, M. A., Brenton, J. D., Chiappinelli, K. B., Martins, F. C., Coukos, G., Drapkin, R., Edmondson, R., Fotopoulou, C., Gabra, H., Galon, J., Gourley, C., Balkwill, F. R. (2015). Rethinking ovarian cancer II: reducing mortality from high-grade serous ovarian cancer. Nature Reviews Cancer, 15(11), 668–679. https://doi.org/10.1038/nrc4019
7. Jayson, G. C., Kohn, E. C., Kitchener, H. C., & Ledermann, J. A. (2014). Ovarian cancer. Lancet, 384(9951), 1376–1388. https://doi.org/10.1016/S0140-6736(13)62146-7
8. Patch, A. M., Christie, E. L., Etemadmoghadam, D., Garsed, D. W., George, J., Fereday, S., Nones, K., Cowin, P., Alsop, K., Bailey, P. J., Kassahn, K. S., Newell, F., Quinn, M. C., Kazakoff, S., Quek, K., Wilhelm-Benartzi, C., Curry, E., Leong, H. S., Australian Ovarian Cancer Study Group, Hamilton, A., … Bowtell, D. D. (2015). Whole-genome characterization of chemoresistant ovarian cancer. Nature, 521(7553), 489–494. https://doi.org/10.1038/nature14410
9. Das PM, Bast RC Jr. Early detection of ovarian cancer. Biomark Med. 2008;2(3):291-303. doi:10.2217/17520363.2.3.291
10. Centers for Disease Control and Prevention. Ovarian cancer statistics. Atlanta (GA): Centers for Disease Control and Prevention; 2025 [cited 2025 Dec 12]. Available from: https://www.cdc.gov/ovarian-cancer/statistics/index.html

11. Wild CP, Weiderpass E, Stewart B, editors. World Cancer Report: Cancer Research for Cancer Prevention. Lyon, France: International Agency for Research on Cancer; 2020. Available from http://publications.iarc.fr/586. Licence: CC BY-NC-ND 3.0 IGO.

12. Cancerfonden. Äggstockscancer – statistik [Internet]. Stockholm: Cancerfonden; [cited 2025 Mar 8]. Available from: https://www.cancerfonden.se/om-cancer/statistik/aggstockscancer

13. European Society of Gynaecological Oncology (ESGO). Ovarian Cancer: Guidelines for Diagnosis, Treatment and Follow-up. 2024 Edition.

14. World Health Organization (WHO). Ovarian Cancer Fact Sheet. 2023.

15. Hankinson SE, Colditz GA, Hunter DJ, Spencer TL, Rosner B, Stampfer MJ. A quantitative assessment of oral contraceptive use and risk of ovarian cancer. Obstet Gynecol. 1992;80(4):708-714.

16. Lycke M, Kristjansdottir B, Sundfeldt K. A multicenter clinical trial validating the performance of HE4, CA125, risk of ovarian malignancy algorithm and risk of malignancy index. Gynecol Oncol. 2018;151(1):159–165.

17. Moore RG, McMeekin DS, Brown AK, et al. A novel multiple marker bioassay utilizing HE4 and CA125 for the prediction of ovarian cancer in patients with a pelvic mass. Gynecol Oncol. 2009;112(1):40–46.

18. Menon U, Gentry-Maharaj A, Burnell M, et al. Ovarian cancer population screening and mortality after long-term follow-up in the UK Collaborative Trial of Ovarian Cancer Screening (UKCTOCS): a randomised controlled trial. Lancet. 2021;397(10290):2182–2193.

19. Blagden SP. Harnessing Pandemonium: The Clinical Implications of Tumor Heterogeneity in Ovarian Cancer. Front Oncol. 2015;5:149. Published 2015 Jun 30. doi:10.3389/fonc.2015.00149

20. Lheureux S, Braunstein M, Oza AM. Epithelial ovarian cancer: Evolution of management in the era of precision medicine. CA Cancer J Clin. 2019;69(4):280-304. doi:10.3322/caac.21559

21. Vaughan S, Coward JI, Bast RC Jr, et al. Rethinking ovarian cancer: recommendations for improving outcomes. Nat Rev Cancer. 2011;11(10):719-725. Published 2011 Sep 23. doi:10.1038/nrc3144

22. Prat J. Ovarian carcinomas: five distinct diseases with different origins, genetic alterations, and clinicopathological features. Virchows Arch. 2012;460(3):237-249. doi:10.1007/s00428-012-1203-5

23. Shih IeM & Kurman RJ. Ovarian tumorigenesis: a proposed model based on morphological and molecular genetic analysis. Am J Pathol. 2004;164(5):1511-1518. doi:10.1016/s0002-9440(10)63708-x

24. Domcke, S., Sinha, R., Levine, D. A., Sander, C., & Schultz, N. (2013). Evaluating cell lines as tumour models by comparison of genomic profiles. Nature Communications, 4, 2126. https://doi.org/10.1038/ncomms3126

25. Cancer Genome Atlas Research Network. Integrated genomic analyses of ovarian carcinoma. Nature. 2011; 474(7353):609–15.

26. López-Reig R, López-Guerrero JA. The Hallmarks of Ovarian Cancer: Proliferation and Cell Growth. J Clin Med. 2020;9(12):4021.

27. Babaier A, Mal H, Alselwi W, Ghatage P. Low-Grade Serous Carcinoma of the Ovary: The Current Status. Diagnostics (Basel). 2022;12(2):458. Published 2022 Feb 10. doi:10.3390/diagnostics12020458

28. Slomovitz B, Gourley C, Carey MS, et al. Low-grade serous ovarian cancer: State of the science. Gynecol Oncol. 2020;156(3):715-725. doi:10.1016/j.ygyno.2019.12.033

29. Prat J; FIGO Committee on Gynecologic Oncology. Staging classification for cancer of the ovary, fallopian tube, and peritoneum. Int J Gynaecol Obstet. 2014;124(1):1-5. doi:10.1016/j.ijgo.2013.10.001

30. Berek JS, Renz M, Kehoe S, Kumar L, Friedlander M. Cancer of the ovary, fallopian tube, and peritoneum: 2021 update. Int J Gynaecol Obstet. 2021;155 Suppl 1(Suppl 1):61-85. doi:10.1002/ijgo.13878

31. Monk BJ, Lorusso D, Fujiwara K, Sehouli J. Optimal Bevacizumab Treatment Strategy in Advanced Ovarian Cancer: A Review. Cancer Treat Rev. 2025;137:102945.

32. Guo H, et al. Cellular Mechanism of Gene Mutations and Potential Therapeutic Targets in Ovarian Cancer. Front Oncol. 2021;11:708795.

33. Feng W, Dean DC, Hornicek FJ, Shi H, Duan Z. Mechanisms of Chemoresistance in Ovarian Cancer. Mol Cancer. 2021;20:54.

34. Pokhriyal R, Hariprasad R, Kumar L. Chemotherapy Resistance in Ovarian Cancer: Mechanisms and Biomarkers. Cancer Drug Resist. 2019;2:620–635.

35. Cutri-French CM, Maher J, Mantzaris MD, et al. CAR-T Cell Therapy in Ovarian Cancer: Where Are We Now? Cancers (Basel). 2024;16(3):678.

36. World Health Organization (WHO). Cervical cancer. Fact sheet. 2023. Available from: https://www.who.int/news-room/fact-sheets/detail/cervical-cancer (accessed Nov 11, 2025).

37. Rosendo-Chalma P, Antonio-Véjar V, Ortiz Tejedor JG, Ortiz Segarra J, Vega Crespo B, Bigoni-Ordóñez GD. The Hallmarks of Cervical Cancer: Molecular Mechanisms Induced by Human Papillomavirus. Biology (Basel). 2024;13(2):77. Published 2024 Jan 27. doi:10.3390/biology13020077

38. Cibula D, Raspollini MR, Planchamp F, et al. ESGO/ESTRO/ESP Guidelines for the management of patients with cervical cancer - Update 2023. Int J Gynecol Cancer. 2023;33(5):649-666. Published 2023 May 1. doi:10.1136/ijgc-2023-004429

39. Wright AA, Howitt BE, Myers AP, et al. Oncogenic mutations in cervical cancer: genomic differences between adenocarcinomas and squamous cell carcinomas of the cervix. Cancer. 2013;119(21):3776-3783. doi:10.1002/cncr.28288

40. Bentivegna E, Gouy S, Maulard A, Chargari C, Leary A, Morice P. Oncological outcomes after fertility-sparing surgery for cervical cancer: a systematic review. Lancet Oncol. 2016;17(6):e240-e253. doi:10.1016/S1470-2045(16)30032-8

41. National Cancer Institute (NCI). PDQ® Adult Treatment Editorial Board. PDQ Cervical Cancer Treatment. Bethesda, MD: National Cancer Institute. Updated May 13 2025. Available from: https://www.cancer.gov/types/cervical/hp/cervical-treatment-pdq (accessed Nov 11, 2025)

42. Bhatla N, Berek JS, Cuello Fredes M, et al. Revised FIGO staging for carcinoma of the cervix uteri. Int J Gynaecol Obstet. 2019;145(1):129-135. doi:10.1002/ijgo.12749

43. Pinto PJJ, Chen MJ, Santos Neto E, et al. Prognostic factors in locally advanced cervical cancer with pelvic lymph node metastasis. Int J Gynecol Cancer. 2022;32(3):239-245. doi:10.1136/ijgc-2021-003140

44. Bhatla N, Aoki D, Sharma DN, Sankaranarayanan R. Cancer of the cervix uteri: 2021 update. Int J Gynaecol Obstet. 2021;155 Suppl 1(Suppl 1):28-44. doi:10.1002/ijgo.13865

45. Mora-Soto N, Morante-Caicedo C, Caicedo-Martínez M, et al. Morbidity of radical surgery and postoperative radiotherapy in cervical cancer. Int J Gynaecol Obstet. 2025;171 Suppl 1(Suppl 1):189-198. doi:10.1002/ijgo.70281

46. Olthof EP, Wenzel HHB, van Maaren MC, et al. Radical hysterectomy or chemoradiotherapy for clinically early-stage cervical cancer with suspicious lymph nodes on imaging: a retrospective cohort study. J Gynecol Oncol. 2025;36(2):e16. doi:10.3802/jgo.2025.36.e16

47. Das M. WHO launches strategy to accelerate elimination of cervical cancer. Lancet Oncol. 2021;22(1):20-21. doi:10.1016/S1470-2045(20)30729-4

48. National Cancer Institute. SEER Cancer Stat Facts: Uterine cancer. Bethesda (MD): National Cancer Institute; [2025; cited 2025 Feb 10]. Available from: https://seer.cancer.gov/statfacts/html/corp.html

49. Brüggmann D, Ouassou K, Klingelhöfer D, Bohlmann MK, Jaque J, Groneberg DA. Endometrial cancer: mapping the global landscape of research. J Transl Med. 2020;18(1):386. Published 2020 Oct 12. doi:10.1186/s12967-020-02554-y

50. Mazidimoradi A, Momenimovahed Z, Khalajinia Z, Allahqoli L, Salehiniya H, Alkatout I. The global incidence, mortality, and burden of uterine cancer in 2019 and correlation with SDI, tobacco, dietary risks, and metabolic risk factors: An ecological study. Health Sci Rep. 2024;7(1):e1835. Published 2024 Jan 25. doi:10.1002/hsr2.1835

51. Webb PM, Aune D, Dossus L. Endometrial cancer: Prevention through control of obesity. In: Wild CP, Weiderpass E, Stewart BW, editors. World Cancer Report: Cancer research for cancer prevention. Lyon (FR): International Agency for Research on Cancer; 2020. 5.11. Available from: https://www.ncbi.nlm.nih.gov/books/NBK606495/?utm_source=chatgpt.com

52. Concin N, Matias-Guiu X, Cibula D, et al. ESGO-ESTRO-ESP guidelines for the management of patients with endometrial carcinoma: update 2025. Lancet Oncol. 2025;26(8):e423-e435. doi:10.1016/S1470-2045(25)00167-6

53. Wright JD, Prest MT, Ferris JS, et al. Projected Trends in the Incidence and Mortality of Uterine Cancer in the United States. Cancer Epidemiol Biomarkers Prev. 2025;34(7):1156-1166. doi:10.1158/1055-9965.EPI-24-1422

54. Feinberg J, Albright B, Black J, et al. Ten-Year Comparison Study of Type 1 and 2 Endometrial Cancers: Risk Factors and Outcomes. Gynecol Obstet Invest. 2019;84(3):290-297. doi:10.1159/000493132

55. Anca-Stanciu MB, Manu A, Olinca MV, et al. Comprehensive Review of Endometrial Cancer: New Molecular and FIGO Classification and Recent Treatment Changes. J Clin Med. 2025;14(4):1385. Published 2025 Feb 19. doi:10.3390/jcm14041385

56. Alexa M, Hasenburg A, Battista MJ. The TCGA Molecular Classification of Endometrial Cancer and Its Possible Impact on Adjuvant Treatment Decisions. Cancers (Basel). 2021;13(6):1478. Published 2021 Mar 23. doi:10.3390/cancers13061478

57. Cancer Genome Atlas Research Network, Kandoth C, Schultz N, et al. Integrated genomic characterization of endometrial carcinoma. Nature. 2013;497(7447):67-73. doi:10.1038/nature12113

58. Guo D, Holmlund C, Henriksson R, Hedman H. The LRIG gene family has three vertebrate paralogs widely expressed in human and mouse tissues and a homolog in Ascidiacea. Genomics. 2004;84(1):157–165. doi: 10.1016/j.ygeno.2004.01.013.

59. Powell AE, Wang Y, Li Y, et al. The pan-ErbB negative regulator Lrig1 is an intestinal stem cell marker that functions as a tumor suppressor. Cell. 2012;149(1):146-158. doi:10.1016/j.cell.2012.02.042

60. Mao F, Holmlund C, Faraz M, et al. Lrig1 is a haploinsufficient tumor suppressor gene in malignant glioma. Oncogenesis. 2018;7:13. doi:10.1038/s41389-017-0012-8

61. Neirinckx V, Hedman H, Niclou SP. Harnessing LRIG1-mediated inhibition of receptor tyrosine kinases for cancer therapy. Biochim Biophys Acta Rev Cancer. 2017 Aug;1868(1):109-116. doi: 10.1016/j.bbcan.2017.02.007. Epub 2017 Mar 1. PMID: 28259645

62. Laederich MB, Funes-Duran M, Yen L, et al. The leucine-rich repeat protein LRIG1 is a negative regulator of ErbB family receptor tyrosine kinases. J Biol Chem. 2004;279(45):47050-47056. doi:10.1074/jbc.M409703200

63. Gur G, Rubin C, Katz M, et al. LRIG1 restricts growth factor signaling by enhancing receptor ubiquitylation and degradation. EMBO J. 2004;23(16):3270-3281. doi:10.1038/sj.emboj.7600342

64. Stutz MA, Shattuck DL, Laederich MB, Carraway KL 3rd, Sweeney C. LRIG1 negatively regulates the oncogenic EGF receptor mutant EGFRvIII. Oncogene. 2008;27(43):5741-5752. doi:10.1038/onc.2008.185

65. Li F, Yang W, Guo D, Hu Z, Xu H, Ye Z. LRIG1 combined with cisplatin enhances bladder cancer lesions via a novel pathway. Oncol Rep. 2011;25(6):1629-1637. doi:10.3892/or.2011.1227

66. Zhang Y, Liu Z, Yu S. Role and mechanism of action of LRIG1 in ovarian cancer cell line and VP16 drug-resistant cell line. Oncol Lett. 2017;14(4):4619-4624. doi:10.3892/ol.2017.6730

67. Billing O, Holmgren Y, Nosek D, Hedman H, Hemmingsson O. LRIG1 is a conserved EGFR regulator involved in melanoma development, survival and treatment resistance. Oncogene. 2021 May;40(21):3707-3718. doi: 10.1038/s41388-021-01808-3. Epub 2021 May 4. PMID: 33947959

68. Faraz M, Herdenberg C, Holmlund C, Henriksson R, Hedman H. A protein interaction network centered on leucine-rich repeats and immunoglobulin-like domains 1 (LRIG1) regulates growth factor receptors. J Biol Chem. 2018;293(9):3421-35. doi:10.1074/jbc.M117.807487.

69. Liu Y, Chen Y, Momin A, Shaner R, Wang E, Bowen NJ, Matyunina LV, Walker LD, McDonald JF, Sullards MC, Merrill AH Jr. Elevation of sulfatides in ovarian

cancer: an integrated transcriptomic and lipidomic analysis including tissue-imaging mass spectrometry. Mol Cancer. 2010 Jul 12;9:186. doi: 10.1186/1476-4598-9-186. PMID: 20624317

70. Devarajan A, Su F, Grijalva V, Yalamanchi M, Yalamanchi A, Gao F, Trost H, Nwokedi J, Farias-Eisner G, Farias-Eisner R, Fogelman AM, Reddy ST. Paraoxonase 2 overexpression inhibits tumor development in a mouse model of ovarian cancer. Cell Death Dis. 2018 Mar 12;9(3):392. doi: 10.1038/s41419-018-0395-2. PMID: 29531225

71. Herdenberg C, Mutie PM, Billing O, Abdullah A, Strawbridge RJ, Dahlman I, et al. LRIG proteins regulate lipid metabolism via BMP signaling and affect the risk of type 2 diabetes. Commun Biol. 2021;4(1):90.

72. Herdenberg C, Hedman H. HYPOTHESIS: Do LRIG Proteins Regulate Stem Cell Quiescence by Promoting BMP Signaling? Stem Cell Rev Rep. 2023 Jan;19(1):59-66. doi: 10.1007/s12015-022-10442-9. Epub 2022 Aug 15.PMID: 35969315 Abdullah et al. (2023)

73. Abdullah A, Herdenberg C, Hedman H. Ligand-specific regulation of transforming growth factor beta superfamily factors by leucine-rich repeats and immunoglobulin-like domains proteins. PLoS One. 2023 Aug 21;18(8):e0289726. doi: 10.1371/journal.pone.0289726. eCollection 2023. PMID: 37603563

74. Abdullah A, Herdenberg C, Hedman H. Netrin-1 functions as a suppressor of bone morphogenetic protein (BMP) signaling. Sci Rep. 2021 Apr 21;11(1):8585. doi: 10.1038/s41598-021-87949-7. PMID: 33883596

75. Krig SR, Frietze S, Simion C, Miller JK, Fry WH, Rafidi H, et al. Lrig1 is an estrogen-regulated growth suppressor and correlates with longer relapse-free survival in ERalpha-positive breast cancer. Mol Cancer Res. 2011;9(10):1406- 17.

76. Lindstrom AK, Ekman K, Stendahl U, Tot T, Henriksson R, Hedman H, et al. LRIG1 and squamous epithelial uterine cervical cancer: correlation to prognosis, other tumor markers, sex steroid hormones, and smoking. Int J Gynecol Cancer. 2008;18(2):312-7.

77. Muller S, Lindquist D, Kanter L, Flores-Staino C, Henriksson R, Hedman H, et al. Expression of LRIG1 and LRIG3 correlates with human papillomavirus status and patient survival in cervical adenocarcinoma. Int J Oncol. 2013;42(1):247-52.

78. Tanemura A, Nagasawa T, Inui S, Itami S. LRIG-1 provides a novel prognostic predictor in squamous cell carcinoma of the skin: immunohistochemical analysis for 38 cases. Dermatol Surg. 2005;31(4):423-30.

79. Sheu JJ, Lee CC, Hua CH, Li CI, Lai MT, Lee SC, et al. LRIG1 modulates aggressiveness of head and neck cancers by regulating EGFR-MAPK-SPHK1 signaling and extracellular matrix remodeling. Oncogene. 2014;33(11):1375-84.

80. Lindquist D, Kvarnbrink S, Henriksson R, Hedman H. LRIG and cancer prognosis. Acta Oncol. 2014;53(9):1135- 42.

81. Kvarnbrink S, Karlsson T, Edlund K, Botling J, Lindquist D, Jirstrom K, et al. LRIG1 is a prognostic biomarker in non-small cell lung cancer. Acta Oncol. 2015;54(8):1113-9.

82. Yang B, Dai C, Tan R, et al. Lrig1 is a positive prognostic marker in hepatocellular carcinoma. Onco Targets Ther. 2016;9:7071-7079. Published 2016 Nov 15. doi:10.2147/OTT.S112534

83. Willis S, Villalobos VM, Gevaert O, Abramovitz M, Williams C, Sikic BI, Leyland-Jones B. Single Gene Prognostic Biomarkers in Ovarian Cancer: A Meta-Analysis. PLoS One. 2016 Feb 17;11(2):e0149183. doi: 10.1371/journal.pone.0149183. eCollection 2016.PMID: 26886260

84. Januchowski R, Sterzyńska K, Zawierucha P, Ruciński M, Świerczewska M, Partyka M, Bednarek-Rajewska K, Brązert M, Nowicki M, Zabel M, Klejewski A. Microarray-based detection and expression analysis of new genes associated with drug resistance in ovarian cancer cell lines. Oncotarget. 2017 Jul 25;8(30):49944-49958. doi: 10.18632/oncotarget.18278. PMID: 28611294

85. Barone A, Linder A, Mateoiu C, Köster Larsen R, Blixt O, Teneberg S, Sundfeldt K. Evaluation of sialyl-lactotetra as a marker for epithelial ovarian tumors. Front Oncol. 2020;10:561888. doi:10.3389/fonc.2020.561888.

86. Engqvist H, Parris TZ, Kovács A, et al. Transcriptomic and Genomic Profiling of Early-Stage Ovarian Carcinomas Associated with Histotype and Overall Survival. Carcinogenesis. 2018;39(7):876–888.

87. Le Page C, Rahimi K, Köbel M, Tonin PN, Meunier L, Portelance L, Bernard M, Nelson BH, Bernardini MQ, Bartlett JMS, Bachvarov D, Gotlieb WH, Gilks B, McAlpine JN, Nachtigal MW, Piché A, Watson PH, Vanderhyden B, Huntsman DG, Provencher DM, Mes-Masson AM. Characteristics and outcome of the COEUR Canadian validation cohort for ovarian cancer biomarkers. BMC Cancer. 2018 Mar 27;18(1):347. doi: 10.1186/s12885-018-4242-8. PMID: 29587661

88. Schmierer, B., Botla, S. K., Zhang, J., Turunen, M., Kivioja, T., & Taipale, J. (2017). CRISPR/Cas9 screening using unique molecular identifiers. Molecular Systems Biology, 13(10), 945. https://doi.org/10.15252/msb.20177834

89. Mitra AK, Davis DA, Tomar S, Roy L, Gurler H, Xie J, Lantvit DD, Cardenas H, Fang F, Liu Y, Loughran E, Yang J, Sharon Stack M, Emerson RE, Cowden Dahl KD, V Barbolina M, Nephew KP, Matei D, Burdette JE. (2015). In vivo tumor growth of high-grade serous ovarian cancer cell lines. Gynecologic Oncology, 138(2), 372–377. doi: 10.1016/j.ygyno.2015.05.040. PMID: 26050922

90. Helland O, Popa M, Vintermyr OK, Molven A, Gjertsen BT, Bjørge L, McCormack E. (2014). First in-mouse development and application of a surgically relevant xenograft model of ovarian carcinoma. PLoS One, 9(3), e89527. doi: 10.1371/journal.pone.0089527. PMID: 24594904

91. Liu J, Lichtenberg T, Hoadley KA, et al. An Integrated TCGA Pan-Cancer Clinical Data Resource to Drive High-Quality Survival Outcome Analytics. Cell. 2018;173(2):400-416.e11. doi:10.1016/j.cell.2018.02.052

92. Wu, X., Hedman, H., Bergqvist, M., Bergström, S., Henriksson, R. et al. (2012) Expression of EGFR and LRIG proteins in oesophageal carcinoma with emphasis on patient survival and cellular chemosensitivity. Acta Oncologica, 51, 69-76. doi:10.3109/0284186X.2011.562239.

93. Yang, H., Yao, J., Yin, J., Wei, X. (2016). Decreased LRIG1 in Human Ovarian Cancer Cell SKOV3 Upregulates MRP-1 and Contributes to the Chemoresistance of VP16. Cancer Biotherapy and Radiopharmaceuticals, 31, 125-132. doi:10.1089/cbr.2015.1970.

94. Morrison, M., Williams, M., Vaught, D. et al. (2016). Decreased LRIG1 in fulvestrant-treated luminal breast cancer cells permits ErbB3 upregulation and increased growth. Oncogene 35, 1143–1152. https://doi.org/10.1038/onc.2015.169.

95. Coffman, L. G., Choi, Y. J., McLean, K., Allen, B. L., di Magliano, M. P., & Buckanovich, R. J. (2016). Human carcinoma-associated mesenchymal stem cells promote ovarian cancer chemotherapy resistance via a BMP4/HH signaling loop. Oncotarget, 7(6), 6916–6932. https://doi.org/10.18632/oncotarget.6870.

96. Fukuda, T., Fukuda, R., Tanabe, R. et al. (2020). BMP signaling is a therapeutic target in ovarian cancer. Cell Death Discov, 6, 139. https://doi.org/10.1038/s41420-020-00377-w.

97. Herrera, B., Inman, G.J. (2009). A rapid and sensitive bioassay for the simultaneous measurement of multiple bone morphogenetic proteins. Identification and quantification of BMP4, BMP6 and BMP9 in bovine and human serum. BMC Cell Biol 10, 20. https://doi.org/10.1186/1471-2121-10-20

98. Peng, J., Yoshioka, Y., Mandai, M., Matsumura, N., Baba, T., Yamaguchi, K., Hamanishi, J., Kharma, B., Murakami, R., Abiko, K., Murphy, S.K. and Konishi, I. (2016), The BMP signaling pathway leads to enhanced proliferation in serous ovarian cancer—A potential therapeutic target. Mol. Carcinog., 55: 335-345. https://doi.org/10.1002/mc.22283

99. Takekuma M, Kasamatsu Y, Kado N, Kuji S, Tanaka A, Takahashi N, et al. The issues regarding postoperative adjuvant therapy and prognostic risk factors for patients with stage I–II cervical cancer: a review. J Obstet Gynaecol Res. 2017;43:617–26.

100. Regionalt Cancercentrum i Samverkan. Livmoderhalscancer och vaginalcancer, nationellt vårdprogram. 2024. Available from: https://kunskapsbanken.cancercentrum.se/diagnoser/livmoderhals-chvaginalcancer/vardprogram/

101. Sevin BU, Nadji M, Lampe B, Lu Y, Hilsenbeck S, Koechli OR, et al. Surgically defined prognostic parameters in patients with early cervical carcinoma: a multivariate survival tree analysis. Cancer. 1996;78(7):1438–46.

102. Alvarez RD, Soong SJ, Kinney WK, Reid GC, Schray MF, Podratz KC, et al. Identification of prognostic factors and risk groups in patients found to have nodal metastasis at the time of radical hysterectomy for early-stage squamous carcinoma of the cervix. Gynecol Oncol. 1989;35(2):130–5.

103. Samverkan R c i (2024) Livmoderhalscancer och vaginalcancer, nationellt v ardprogram. in, Regionalt cancercentrum i samverkan. https://kunskapsbanken.cancercentrum.se/diagnoser/livmoderhals-ochvaginalcancer/vardprogram/

104. Klaes R, Friedrich T, Spitkovsky D, Ridder R, Rudy W, Petry U, et al. Overexpression of p16(INK4A) as a specific marker for dysplastic and neoplastic epithelial cells of the cervix uteri. Int J Cancer. 2001;92:276–84.

105. Sano T, Oyama T, Kashiwabara K, Fukuda T, Nakajima T. Expression status of p16 protein is associated with human papillomavirus oncogenic potential in cervical and genital lesions. Am J Pathol. 1998;153:1741–8.

106. Zhang J, Zhou Y, Huang W, Zuo L, Zhu Y, Zhang W, et al. Leucine-rich repeats and immunoglobulin-like domains protein 1 and fascin actin-bundling protein 1 expression in nonsmall cell lung cancer. J Cancer Res Ther. 2016;12 Suppl:C248–51.

107. Hedman H, Henriksson R. LRIG inhibitors of growth factor signalling: double-edged swords in human cancer? Eur J Cancer. 2007;43(4):676–82.

108. Karlsson T, Mark EB, Henriksson R, Hedman H. Redistribution of LRIG proteins in psoriasis. J Invest Dermatol. 2008;128:1192–5.

109. de Melo, A.L.L., et al., Single-molecule array assay reveals the prognostic impact of plasma LRIG1 in ovarian carcinoma. Acta Oncol, 2022. 61(11): p. 1425-1433.

110. Nilsson J, Starefeldt A, Henriksson R, Hedman H. LRIG1 protein in human cells and tissues. Cell Tissue Res. 2003 Apr;312(1):65-71. doi: 10.1007/s00441-003-0697-1. Epub 2003 Mar 18.PMID: 12684867

111. Uhlén M, Fagerberg L, Hallström BM, Lindskog C, Oksvold P, Mardinoglu A, et al. Tissue-based map of the human proteome. Science. 2015;347(6220):1260419. doi:10.1126/science.1260419.

112. Human Protein Atlas. LRIG1 in ovarian cancer – survival analysis. Available from: https://v22.proteinatlas.org/ENSG00000144749-LRIG1/pathology/ovarian%2Bcancer

113. Yi W, Haapasalo H, Holmlund C, Järvelä S, Raheem O, Bergenheim AT, et al. Expression of leucine-rich repeats and immunoglobulin-like domains (LRIG) proteins in human ependymoma relates to tumor location, WHO grade, and patient age. Clin Neuropathol. 2009;28(1):21-7. doi:10.5414/NPP28021.

114. Singer G, Oldt R 3rd, Cohen Y, Wang BG, Sidransky D, Kurman RJ, Shih IeM. Mutations in BRAF and KRAS characterize the development of low-grade ovarian serous carcinoma. J Natl Cancer Inst. 2003 Mar 19;95(6):484-6. doi: 10.1093/jnci/95.6.484. PMID: 12644542

115. Manning-Geist B, Gordhandas S, Liu YL, Zhou Q, Iasonos A, Da Cruz Paula A, Mandelker D, Long Roche K, Zivanovic O, Maio A, Kemel Y, Chi DS, O'Cearbhaill RE, Aghajanian C, Weigelt B, Chui MH, Grisham RN. MAPK Pathway Genetic Alterations Are Associated with Prolonged Overall Survival in Low-Grade Serous Ovarian Carcinoma. Clin Cancer Res. 2022 Oct 14;28(20):4456-4465. doi: 10.1158/1078-0432.CCR-21-4183. PMID: 35443055

116. Takeda H, Wei Z, Koso H, Rust AG, Yew CC, Mann MB, Ward JM, Adams DJ, Copeland NG, Jenkins NA. Transposon mutagenesis identifies genes and evolutionary forces driving gastrointestinal tract tumor progression. Nat Genet. 2015 Feb;47(2):142-50. doi: 10.1038/ng.3175. Epub 2015 Jan 5. PMID: 25559195

117. Gipson GR, Goebel EJ, Hart KN, Kappes EC, Kattamuri C, McCoy JC, Thompson TB. Structural perspective of BMP ligands and signaling. Bone. 2020 Nov;140:115549. doi: 10.1016/j.bone.2020.115549. Epub 2020 Jul 27. PMID: 32730927

118. Oliver-Perez MR, Padilla-Iserte P, Arencibia-Sanchez O, Martin-Arriscado C, Muruzabal JC, Diaz-Feijóo B, et al. Lymphovascular Space Invasion in Early-Stage Endometrial Cancer (LySEC): Patterns of Recurrence and Predictors. A Multicentre Retrospective Cohort Study of the Spain Gynecologic Oncology Group. Cancers (Basel). 2023;15(9).

119. Ghasimi S, Haapasalo H, Eray M, Korhonen K, Brännström T, Hedman H, Andersson U. Immunohistochemical analysis of LRIG proteins in meningiomas: correlation between estrogen receptor status and LRIG expression. J Neurooncol. 2012;108(3):435-41. doi:10.1007/s11060-012-0856-x.

120. Razumova Z, Oda H, Govorov I, et al. The Prognostic Role of LRIG Proteins in Endometrial Cancer. Cancers (Basel). 2021;13(6):1361. Published 2021 Mar 17. doi:10.3390/cancers13061361

121. Gargiulo G, Serresi M, Cesaroni M, Hulsman D, van Lohuizen M. In vivo shRNA screens in solid tumors. Nat Protoc. 2014;9(12):2880-2902. doi:10.1038/nprot.2014.185